Advances in Stochastic Medical Image Registration

Vooruitgang in de stochastische medische beeldregistratie

Proefschrift

ter verkrijging van de graad van doctor aan de
Erasmus Universiteit Rotterdam
op gezag van de
rector magnificus

Prof.dr. H.A.P. Pols

en volgens besluit van het College voor Promoties.

De openbare verdediging zal plaatsvinden op
dinsdag 15 december 2015 om 11:30 uur

door

Wei Sun

geboren te Xi'an, China

Erasmus University Rotterdam

Promotiecommissie

Promotor: **Prof.dr. W.J. Niessen**

Overige leden: **Dr.ir. J.G. Bosch**

                  Dr.ir. F.M. Vos

   **Prof.dr. D. Rueckert**

Copromotor: **Dr.ir. S. Klein**

To my family

Colophon
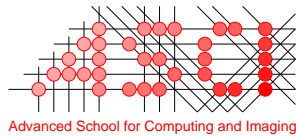
Advanced School for Computing and Imaging

Contents

Introduction

M edical imaging plays an indispensable role in clinical research, biomedical research, and clinical care. It enables the physicians and researchers to inspect the anatomy and function of the human body, in a non- or minimally invasive manner, and to detect and inspect pathologies. Medical imaging is therefore widely applied, e.g., in disease detection, diagnosis, therapy planning, guidance of intervention and therapy monitoring and follow-up. Image analysis plays an increasingly important role in medical imaging, e.g., for the automated extraction of quantitive information relevant for supporting diagnosis or to construct anatomical and functional models for therapy planning and guidance. Often multiple imaging datasets are available, in which case image registration can be used to spatially relate imaging data. Registration can for example be used to align image data sets acquired at different time points (e.g., dynamic lung computed tomography (CT) imaging), from different subjects (e.g., intersubject brain study)), or from different imaging modalities (e.g. functional of the imaging of the heart with magnetic resonance imaging (MRI) or single-photon emission computed tomography (SPECT) complemented with anatomical imaging with CT). Figure 1.1 shows a simple example of multimodal registration on MRI brain images using rigid transformation. The registration process estimates a rigid transformation required to align the brain structures in both scans. In this thesis, we present novel methods for performing such image registrations, with the aim to improve accuracy, robustness, and speed compared with existing methods.
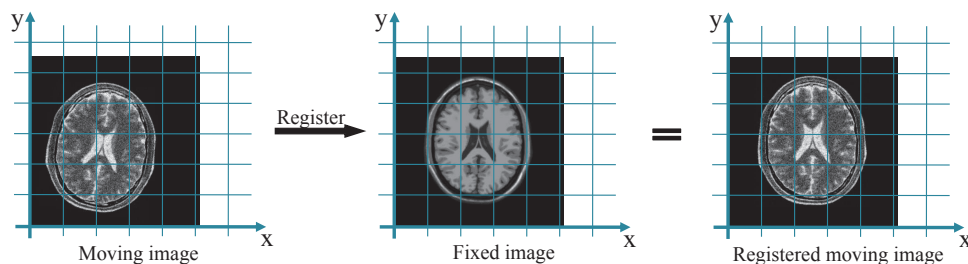

**Figure 1.1.** Example of multimodal brain MRI registration.
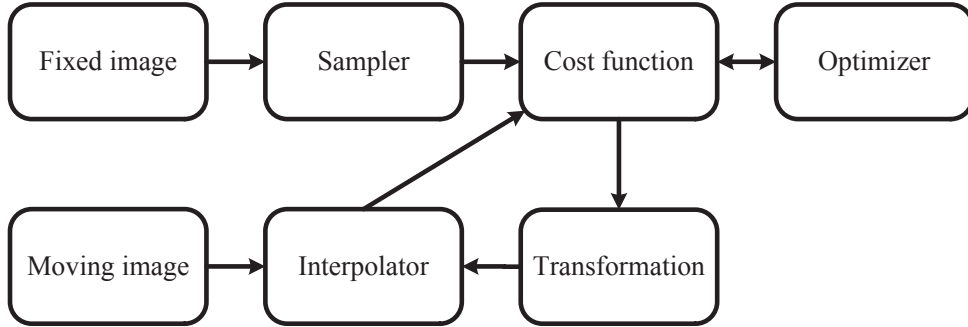
Figure 1.2. Framework for intensity-based image registration.

1.1   Background

There exists a large body of literature on image registration, and extensive surveys on the subject can be found in literature [20, 35, 61, 94, 107]. Generally, feature-based and intensity-based algorithms are distinguished, which use either high-level feature information or raw image intensities, respectively. In this thesis, we restrict our attention to intensity-based methods, since they are most widely used.

Intensity-based image registration is typically formulated as an optimization problem, which aims to find the optimal spatial transformation(s) by minimizing a cost function that measures the dissimilarity between two or more images. Figure 1.2 provides a schematic overview of the registration framework, explained below.

Let $F(\boldsymbol{x}) : \Omega_F \subset \mathbb{R}^D \to \mathbb{R}$ and $M(\boldsymbol{x}) : \Omega_M \subset \mathbb{R}^D \to \mathbb{R}$ denote the D-dimensional *fixed image* and *moving image* where $\boldsymbol{x}$ represents an image coordinate, and Ω_F and Ω_M are the domains of the fixed and moving images, respectively. During the registration process, the moving image $M(\boldsymbol{x})$ is gradually transformed to fit the fixed image $F(\boldsymbol{x})$. The *transformation* is defined as a mapping from the fixed image to the moving image, i.e. $\mathbf{T}(\boldsymbol{\mu}, \boldsymbol{x}) : \mathbb{R}^P \times \Omega_F \to \Omega_M$ where $\boldsymbol{\mu} \in \mathbb{R}^P$ is the parameter vector of the transformation model and P is the number of transformation parameters. $\mathbf{T}(\boldsymbol{\mu}, \boldsymbol{x})$ could be a translation, rigid, affine or nonrigid (e.g., B-spline) transformation model. Different nonrigid transformation models have been summarized in [36]. To acquire samples from the fixed image, i.e., voxel coordinates $\boldsymbol{x}_i \in \Omega_F$ with corresponding image values $F(\boldsymbol{x}_i)$, an image *sampler* is employed. According to different sampling strategies, a full set or a subset of samples is extracted from the image data. Computation time can be reduced by using a subset of image data. In [47], a more detailed description of different sampling strategies is provided. During the registration procedure, the sampled coordinates $\boldsymbol{x}_i \in \Omega_F$ are transformed by $\mathbf{T}(\boldsymbol{\mu}, \boldsymbol{x}_i)$ to obtain the corresponding locations in the moving image M. The transformed coordinate is usually located at an off-grid position. Therefore, an image *interpolator* is used to calculate the intensity value at that location, $M(\mathbf{T}(\boldsymbol{\mu}, \boldsymbol{x}_i))$, by interpolation from the voxel values in its neighbourhood. Extensive surveys of interpolation methods are presented in [54, 65, 105]. The quality of alignment is defined by a *cost function* $\mathcal{C}$

which measures the dissimilarity between the fixed image $F(\boldsymbol{x})$ and the transformed moving image $M(\mathbf{T}(\boldsymbol{\mu}, \boldsymbol{x}))$. Examples of $\mathcal{C}$ are the sum of squared differences (SSD), normalized correlation coefficient (NCC), and mutual information [21]. For instance, if SSD is used as similarity measure, the cost function $\mathcal{C}$ is formulated as:

$$\mathcal{C}\left(\boldsymbol{\mu}, \Omega_F\right) = \frac{1}{|\Omega_F|} \sum_{\boldsymbol{x}_i \in \Omega_F} \left(F(\boldsymbol{x}_i) - M\left(\mathbf{T}(\boldsymbol{\mu}, \boldsymbol{x}_i)\right)\right)^2. \tag{1.1}$$

The registration problem is defined as:

$$\hat{\boldsymbol{\mu}} = \arg\min_{\boldsymbol{\mu}} \mathcal{C}\left(\boldsymbol{\mu}, \Omega_F\right). \tag{1.2}$$

Since Eq. (1.2) has no closed-form solution for many realistic tasks, an iterative *optimization* procedure is commonly applied to find the optimal set of parameters $\hat{\boldsymbol{\mu}}$. Well-known instances of such optimizers are gradient descent [73], quasi-Newton [25], and nonlinear conjugate gradient [22]. Finally, in many registration methods a *multiresolution* strategy (not shown in Figure 1.2) is adopted to first achieve rough alignment, which is subsequently refined.

The choice of numerical optimization procedure has a major impact on the performance of the image registration algorithm. Most registration algorithms use iterative gradient-based techniques, in which the derivative of the cost function with respect to the transformation parameters is used to define the search direction in parameters space. We can define an iterative optimization strategy to find the optimal set of parameters $\hat{\boldsymbol{\mu}}$,

$$\boldsymbol{\mu}_{k+1} = \boldsymbol{\mu}_k - \gamma_k \boldsymbol{d}_k, \quad k = 1, 2, \ldots, K, \quad \hat{\boldsymbol{\mu}} = \boldsymbol{\mu}_K \tag{1.3}$$

where $\boldsymbol{d}_k$ represents the "optimization direction" at iteration k, and γ_k controls the step size along $\boldsymbol{d}_k$. In gradient-based optimization methods, the definition of $\boldsymbol{d}_k$ is based on the derivative of the cost function with respect to $\boldsymbol{\mu}$, $\partial\mathcal{C}/\partial\boldsymbol{\mu}$.

In [48] the performances of eight optimization methods were evaluated for image registration: gradient descent (with two different step size selection algorithms) [73], quasi-Newton [25], nonlinear conjugate gradient [22], Kiefer-Wolfowitz [41], simultaneous perturbation [96], Robbins-Monro (RM) [82], and evolution strategy [32]. The first four methods evaluated in [48] belong to the deterministic category where the derivative of the cost function is calculated in a deterministic manner. The second three methods are stochastic gradient descent (SGD) optimizers where only approximated gradients of the cost function are needed during the optimization. The last method can be considered as a stochastic optimizer but it does not depend on gradient information of the cost function. Through a systematic comparison, the RM optimizer achieved competitive performance among deterministic and stochastic candidates in terms of computation time, registration accuracy and robustness. In [48], the RM method was implemented by using in each iteration a newly selected random subset of image data to calculate the cost function gradient. This is in contrast to the deterministic optimization methods, in which a fixed set of image samples is used throughout the optimization. In this thesis we focus on the RM method. So far, SGD methods based on the RM have been widely applied in many registration problems, e.g., [7, 24, 28, 42, 49, 66, 69, 91, 97, 118].

1.2 Stochastic gradient descent based image registration

Since we focus on SGD based image registration methods in this thesis, below we introduce this type of registration algorithm in more detail. SGD optimization is described by the following iterative update process:

$$\boldsymbol{\mu}_{k+1} = \boldsymbol{\mu}_k - \gamma_k \tilde{\boldsymbol{g}}_k, \tag{1.4}$$

where $\tilde{\boldsymbol{g}}_k$ is a stochastic approximation of the cost function derivative $\partial \mathcal{C}/\partial \boldsymbol{\mu}$, evaluated at the current recovered transformation parameters $\boldsymbol{\mu}_k$, and γ_k is a scalar gain factor that controls the step size along $\tilde{\boldsymbol{g}}_k$. To guarantee the convergence of SGD optimization, a common choice of γ_k is

$$\gamma_k = a/(k + A)^{\alpha}, \tag{1.5}$$

where $a > 0$, $A \geq 1$, and $0 < \alpha \leq 1$ are user-defined parameters. Kushner and Yin [52] proved that $\alpha = 1$ gives a theoretically optimal rate of convergence when $k \to \infty$.

In [48], the stochastic approximation $\tilde{\boldsymbol{g}}_k$ was calculated by evaluating $\partial \mathcal{C}/\partial \boldsymbol{\mu}$ on a small random subset $\widetilde{\Omega}_F^k \subset \Omega_F$ of image samples, hence reducing the computation time per iteration. This subset $\widetilde{\Omega}_F^k$ should be randomly refreshed in each iteration k, to make the approximation stochastic. We thus can write:

$$\tilde{\boldsymbol{g}}_k = \tilde{\boldsymbol{g}}(\boldsymbol{\mu}_k, \widetilde{\Omega}_F^k) = \frac{\partial \mathcal{C}}{\partial \boldsymbol{\mu}}(\boldsymbol{\mu}_k, \widetilde{\Omega}_F^k) \approx \frac{\partial \mathcal{C}}{\partial \boldsymbol{\mu}}(\boldsymbol{\mu}_k, \Omega_F). \tag{1.6}$$

For example, if we choose SSD as a cost function $\mathcal{C}$ (see Eq. (1.1)), $\tilde{\boldsymbol{g}}_k$ is computed as:

$$\tilde{\boldsymbol{g}}_k = \frac{2}{|\widetilde{\Omega}_F^k|} \sum_{\boldsymbol{x}_i \in \widetilde{\Omega}_F^k} \left(F(\boldsymbol{x}_i) - M\left(\mathbf{T}(\boldsymbol{\mu}_k, \boldsymbol{x}_i)\right) \right) \left(\frac{\partial \mathbf{T}}{\partial \boldsymbol{\mu}}\Big|_{(\boldsymbol{\mu}_k, \boldsymbol{x}_i)} \right)^T \left(\frac{\partial M}{\partial \boldsymbol{x}}\Big|_{\mathbf{T}(\boldsymbol{\mu}_k, \boldsymbol{x}_i)} \right). \tag{1.7}$$

Although the SGD-based registration has been widely used in medical image analysis, there are still several aspects which restrict its application. First, local minima in the cost function may cause the optimization to converge to a suboptimal solution. This is a common problem in gradient-based optimization methods (not only SGD) and is often the cause of misregistration. Second, in nonrigid image registration tasks, the computation time remains a bottleneck in many applications, especially in large scale clinical and population-based studies, or if real-time image registration is required, e.g., for image guidance in interventions, etc. Third, for the SGD optimization itself, the issue of selecting a good sequence of step size γ_k is also a major challenge in practice [52]. If the step size γ_k is chosen too small, the minimizing process of the cost function will be too slow and easily get stuck at an early stage. If γ_k is selected too large, the noise during the stochastic optimization will become too large and the reliability of the optimization cannot be guaranteed.

1.3   Purpose

As shown in Figure 1.2, and as described above, the registration framework consists of different processing components. The performance of each component may directly affect the result of image registration in terms of registration accuracy, robustness, transformation smoothness and computation time. This thesis presents several advances in stochastic (SGD-based) medical image registration, aiming to improve registration accuracy, robustness and speed. Specifically we address differerent multiresolution strategies, transformation models, and optimization methods.

1.4   Overview

Below we provide a brief outline of each chapter:

Chapter 2 Multiresolution strategies are commonly used in nonrigid registration to avoid local minima in the optimization space. Generally, a step-by-step hierarchical approach is adopted, in which the registration starts on a level with reduced complexity (downsampled images, global transformations), then continuing to levels with increased complexity, until the finest level is reached. In Chapter 2 we propose two alternative multiresolution strategies, in which different resolution levels are considered simultaneously instead of subsequently. By combining different multiresolution strategies for imaging data and transformation model, a 3×3 multiresolution scheme is defined, including both existing and novel methods. In extensive experiments we evaluate the different existing hierarchical methods, finding that some of the novel simultaneous multiresolution approaches outperform conventional approaches.

Chapter 3 Instead of stacking B-spline transformation levels in a redundant fashion, wavelet analysis leads to a unique decomposition of a signal into its coarse- and fine-scale components. Potentially, this could be useful for image registration. Therefore, we investigated whether a wavelet-based free-form deformation (FFD) model has advantages over other models for nonrigid image registration in Chapter 3. We used a B-spline based wavelet and this wavelet is expressed as a linear combination of B-spline basis functions. Derived from the original B-spline function, this wavelet is smooth, differentiable, and compactly supported. The basis functions of this wavelet are orthogonal across scales in Sobolev space. The wavelet transformation is essentially a (linear) reparameterization of the B-spline transformation model. Experiments show that wavelet based registration leads to smoother deformation fields than traditional B-splines based registration, while at the same time achieving better accuracy.

Chapter 4 In most literature on FFD based registration, a B-spline transformation model is the method of choice. B-splines become smoother with increasing spline order. However, a higher-order B-spline requires a larger support region involving more control points, which means higher computational cost. In general, the third-order B-spline is considered as a good compromise between spline smoothness and computational cost. A lower-order function is seldomly used to

construct the transformation model for registration since it is less smooth. In Chapter 4 we investigate whether lower-order B-spline functions can be utilized for more efficient registration, while preserving smoothness of the deformation by using a novel random perturbation technique in combination with an SGD optimization scheme. Experiments demonstrate that the novel randomly perturbed free-form deformation (RPFFD) approach improves the registration accuracy and transformation smoothness. Meanwhile, lower-order RPFFD methods reduce the computational cost substantially.

Chapter 5 Due to the image content and transformation model, there are usually many local minima in the optimization landscape of a typical registration problem. To avoid local minima and reach the global optimum, smoothing the cost function would be desirable. In Chapter 5, we investigate the use of a randomized smoothing (RS) technique for the SGD based registration, to effectively smooth the cost function. In this approach, Gaussian noise is added to the transformation parameters prior to computing the cost function gradient in each iteration of the SGD optimizer. The RS technique is applied to translation, rigid, affine and B-spline transformation models. Experiments demonstrate the effectiveness of the novel RS technique for stochastic image registration on translation, rigid, affine and nonrigid B-spline transformations in terms of registration accuracy and robustness.

Chapter 6 In SGD based registration algorithms, the optimization step size is an important parameter. With larger step sizes, the risk of getting stuck at the early stage is reduced, and convergence rate might be accelerated, but precision after a finite number of iterations is reduced. To mitigate the last effect, Polyak and Juditsky have proposed an iterate averaging technique, and have proven that the averaged sequence converges to its limit at an optimal rate under certain assumptions [79]. Based on this technique, we developed an averaged SGD (Avg-SGD) optimization method for image registration. We evaluated the method in rigid and nonrigid image registration applications, and compared it to state-of-the-art conventional SGD methods. Experiments on simulated 2D brain MRI data and real 3D lung CT scans demonstrate the effectiveness of the Avg-SGD method in terms of convergence rate and registration precision.

Chapter 7 We conclude the thesis with a brief summary, a discussion of general strengths and limitations of our work, and suggestions for future research.

Simultaneous multiresolution strategies for nonrigid image registration

Abstract — Multiresolution strategies are commonly used in the nonrigid registration to avoid local minima in the optimization space. Generally, a step-by-step hierarchical approach is adopted, in which the registration starts on a level with reduced complexity (downsampled images, global transformations), then continuing to levels with increased complexity, until the finest level is reached. In this chapter we propose two alternative multiresolution strategies for both the data model and transformation model, in which different resolution levels are considered simultaneously instead of subsequently. By combining the different strategies for data and transformation, we systematically define 3×3 multiresolution schemes, including both existing and novel methods. Experiments on 10 pairs of CT lung datasets showed that the best performing strategy resulted in a reduction of the upper quartile of the mean target registration error from 2 mm to 1.5 mm, compared with the conventionally hierarchical multiresolution method, while achieving smoother deformations. Experiments with intersubject registration of 18 3D T1-weighted MRI brain scans confirmed that simultaneous multiresolution strategies produce more accurate registration results (median of mean overlap increased from 0.55 to 0.57) and smoother deformation fields than the traditionally hierarchical method. Evaluation of robustness indicated that the largest differences in accuracy between methods are observed for structures with a relatively large initial misalignment.

2.1   Introduction

Nonrigid image registration is critical to many tasks in medical image analysis [20, 35, 61, 107]. In this work we focus on intensity-based registration with a parametric transformation model (using B-splines for example) [85]. In such methods, the optimal parameter values of the transformation model are determined by an iterative numerical optimization procedure, which maximizes the similarity between the images. It is a well-known problem that undesired local minima may exist in the optimization space. Also, when the number of parameters is very large (i.e., a high transformation complexity is allowed in the nonrigid registration), the image information alone may not be sufficient to clearly indicate the optimum. Therefore, nonrigid image registration is often considered as an ill-posed optimization problem [27].

To guide optimization in nonrigid registration, various multiresolution strategies have been proposed, which utilize a coarse-to-fine optimization. An extensive survey of different multiresolution strategies is provided by Lester and Arridge [55]. In this survey these strategies are classified into three groups: increasing data complexity, increasing warp complexity, and increasing model complexity. One or more of these strategies are used in many of the existing methods. For example, in case of a B-spline transformation model [85], commonly the coarsest B-spline grid is first applied to the most blurred image in the initial resolution level of the registration. In subsequent resolution levels, the B-spline control point grid is refined and a less blurred image is used, until the finest grid spacing is reached and the original non-smoothed image is used.

In comparison to such a step-by-step hierarchical strategy, simultaneous multiresolution strategies could have advantages. If the low and high resolution levels of data are combined to guide the optimization, large-scale and small-scale image information can be considered simultaneously. Similarly, a simultaneous multiresolution strategy for the transformation model could be employed to distribute the whole deformation to the different resolution levels of the transformation model. Ideally, large deformations should be represented by a coarser transformation level, and remaining smaller deformations should be captured by the finer transformation levels. A number of methods with simultaneous multiresolution ideas have been proposed. Van Stralen and Pluim [116] encoded the image dissimilarity from different resolutions simultaneously into a directed acyclic graph (DAG), and then used dynamic programming to find the best subgraph of DAG. Somayajula *et al.* [92] considered image features from different resolution levels simultaneously, by using a feature vector derived from multiresolution information at each voxel in the registration. Most recently, Shi *et al.* [90] added a L^1- norm sparsity term to a multi-level free-form deformation (FFD) model to capture motion discontinuities more robustly. However, to the best of our knowledge there is no literature which extensively compares the performances of different mutiresolution strategies.

In this chapter, we define three multiresolution concepts, named Hierarchical (H), Simultaneous (S) and Hierarchically Simultaneous (HS), respectively. These concepts can be implemented both for the image data (D) and for the transformation model (T). Table 2.1 provides an overview of the resulting strategies, which will be explained

in detail in Section 6.2.

Table 2.1. Multiresolution strategies for image data and transformation. 3×3 combinations of multiresolution methods can be constructed based on these multiresolution strategies, which will result in TH-DH, TH-DS, TH-DHS, TS-DH, TS-DS, TS-DHS, THS-DH, THS-DS, and THS-DHS registration methods (see Section 6.2 for precise explanation).

- Image data
  - DH: start with the most blurred image, then a less blurred image, and so on, until the original image resolution;
  - DS: use the entire scale stack of different resolutions at once;
  - DHS: start with the most blurred image, then use the most blurred and a less blurred images, and so on, until the entire scale stack is used.

- Transformation model
  - TH: start with the coarsest transformation level, next phase use a finer transformation, and so on, until the finest transformation is used;
  - TS: optimize the coarse and fine deformations simultaneously;
  - THS: start with the coarsest transformation level, then add a finer scale while still optimizing the coarsest scale, and so on, until all scales are being optimized simultaneously.

Based on these strategies, we can construct 3×3 multiresolution combinations. In addition, we propose two slightly different ways to implement the DS and DHS strategies ('Sum' and 'Union'). Excluding duplicate methods (see Section 2.2.3), this results in a total of 10 different methods, which were evaluated and compared in this study. The traditional multiresolution method which is still most commonly used, is naturally included in this systematic study and can hence effectively be compared with the other multiresolution strategies.

We implemented all methods using the FFD with B-splines [85]. FFD has been successfully applied to many registration applications [36, 122]. Compared to other registration methods, FFD produced competitive results [44, 69]. In our experiments, we used publicly available CT (computed tomography) lung and T1-weighted MRI (magnetic resonance imaging) brain data in the evaluation study. The performances of the different multiresolution strategies were evaluated in terms of both registration accuracy and smoothness of transformation. On lung data, we used mean of target registration error (mTRE) based on widely distributed landmarks as the measure of the registration accuracy. To measure the accuracy of the brain data, overall mean

overlap (MO) of 84 manually annotated labels was used. Because many small tissues are labeled in these brain data, the overall mean overlap is a reliable measure of registration accuracy [83]. On both lung and brain data, the determinant of the spatial Jacobian (D_{SJ}) was used to measure the smoothness of the estimated transformation. A preliminary version of this work was reported in [98], but only five lung data sets were used to evaluate the performance, and the results were only evaluated in terms of accuracy.

This chapter is organized as follows. Section 6.2 explains the newly proposed multiresolution methods. Section 2.3 provides some implementation details. In Section 6.3, experiments are conducted to evaluate the performances of different combinations of multiresolution strategies. The experimental results are presented in Section 6.4. In Section 6.5 the experimental results are interpreted and discussed. Finally, the conclusions are drawn in the last section.

2.2   Method

We consider D-dimensional fixed and moving images $F(\mathbf{x}) : \Omega_F \subset \mathcal{R}^D \to \mathcal{R}$ and $M(\mathbf{x}) : \Omega_M \subset \mathcal{R}^D \to \mathcal{R}$, where $\mathbf{x} \in \mathcal{R}^D$ represents the image coordinates.

In nonrigid image registration, a nonrigid transformation $\mathbf{T}_{\boldsymbol{\mu}}$ is gradually recovered by minimizing the dissimilarity $\mathcal{C}$ between the fixed image and the deformed moving image:

$$\hat{\boldsymbol{\mu}} = \arg\min_{\boldsymbol{\mu}} \mathcal{C}(F, M \circ \mathbf{T}_{\boldsymbol{\mu}}), \qquad (2.1)$$

where $\boldsymbol{\mu}$ denotes the parameter vector of the transformation model $\mathbf{T}$, and $\mathbf{T}_{\boldsymbol{\mu}}(\mathbf{x}) : \Omega_F \to \Omega_M$. The dimensionality of the optimization space, which is reflected by the length of the vector $\boldsymbol{\mu}$, is usually very high in nonrigid registration. To simplify the notation, we denote $M_{\boldsymbol{\mu}}(\mathbf{x}) = M \circ \mathbf{T}_{\boldsymbol{\mu}}(\mathbf{x}) = M(\mathbf{T}_{\boldsymbol{\mu}}(\mathbf{x}))$.

2.2.1   Multiresolution Strategies for Image Data

To generate multiresolution data, we convolve the original fixed and moving images with a Gaussian kernel s of varying widths:

$$\begin{cases} F(\mathbf{x}, s) = G_s * F(\mathbf{x}) \\ M(\mathbf{x}, s) = G_s * M(\mathbf{x}) \end{cases}, \qquad (2.2)$$

where G_s denotes the Gaussian kernel, with standard deviation σ_s, which decreases with increasing s.

Using the above notation, we can introduce different multiresolution strategies for the image data by making the cost function $\mathcal{C}$ dependent on the resolution level p of the registration process. In the following equations, we define the cost functions

that correspond to DH, DS and DHS:

$$\text{DH:} \qquad \mathcal{C}^p = \mathcal{C}(F(\mathbf{x}, p), M_{\boldsymbol{\mu}}(\mathbf{x}, p)), \tag{2.3}$$

$$\text{DS:} \qquad \begin{cases} \text{Sum: } \mathcal{C}^p = \sum_{s=1}^{S} \mathcal{C}(F(\mathbf{x}, s), M_{\boldsymbol{\mu}}(\mathbf{x}, s)), \\ \text{Union: } \mathcal{C}^p = \mathcal{C}(\bigcup_{s=1}^{S}(F(\mathbf{x}, s), M_{\boldsymbol{\mu}}(\mathbf{x}, s))), \end{cases} \tag{2.4}$$

$$\text{DHS:} \qquad \begin{cases} \text{Sum: } \mathcal{C}^p = \sum_{s=1}^{p} \mathcal{C}(F(\mathbf{x}, s), M_{\boldsymbol{\mu}}(\mathbf{x}, s)), \\ \text{Union: } \mathcal{C}^p = \mathcal{C}(\bigcup_{s=1}^{p}(F(\mathbf{x}, s), M_{\boldsymbol{\mu}}(\mathbf{x}, s))), \end{cases} \tag{2.5}$$

where S denotes the number of resolution levels, $p \in [1, S]$ represents the current resolution level of the registration process, $\mathcal{C}^p$ is the cost function at registration level p, and the Sum and Union represent two different ways to integrate image information from multiple resolution levels. Equation (2.3) reflects that in the traditionally used hierarchical strategy DH in which only one image resolution level is considered at a time in each registration resolution level p. In DS, all image resolution levels are used simultaneously. In DHS, the image resolution levels up to level p are used simultaneously.

If multi-level data are considered simultaneously, as in DS and DHS, it has to be decided how to integrate the information from the different image scales into a single cost function. In this work, we investigate two straightforward approaches, called Sum and Union. In the Sum definition, the cost function is calculated for each resolution level separately, and the overall cost is defined as their sum. In the Union definition, a single cost function is calculated by pooling the fixed-moving intensity pairs $(F(\mathbf{x}, s), M_{\boldsymbol{\mu}}(\mathbf{x}, s))$ from the coarse and fine resolution levels. For sum of squared intensity differences (SSD), the Sum and Union definitions become equivalent. However, if normalized correlation coefficient (NCC) or mutual information (MI) is chosen as similarity metric, the Sum and Union approaches lead to different definitions of $\mathcal{C}^p$. Figure 2.1 illustrates the DH, DS and DHS strategies, when three resolution levels are used.

2.2.2 Multiresolution Strategies for the Transformation

A FFD transformation model using B-splines [85] can be defined as follows:

$$\mathbf{T}_{\boldsymbol{\mu}}(\mathbf{x}) = \mathbf{x} + \sum_{\mathbf{x}_i \in I_{\mathbf{x}}} \mathbf{c}_i \beta^r((\mathbf{x} - \mathbf{x}_i)/g), \tag{2.6}$$

where $\mathbf{x}_i$ represents a control point of the B-spline grid, $I_{\mathbf{x}}$ is the set of control points within a compact support region of the B-splines around $\mathbf{x}$, β^r represents the rth order multidimensional B-spline polynomial, g is the spacing between grid points, $\mathbf{c}_i$ is the B-spline coefficient vector of control point $\mathbf{x}_i$, and the parameter vector $\boldsymbol{\mu}$ is formed by the elements of all $\mathbf{c}_i$ ($\boldsymbol{\mu} = \{\mathbf{c}_i\}_{\mathbf{x}_i \in I}$). By making the definition of the transformation model dependent on the resolution level p of the registration, we can define the conventional hierarchical strategy TH, the simultaneous multiresolution strategy TS, and the hierarchically simultaneous multiresolution strategy THS. In TS and THS a dependence on s is also introduced, in order to couple the image scale to
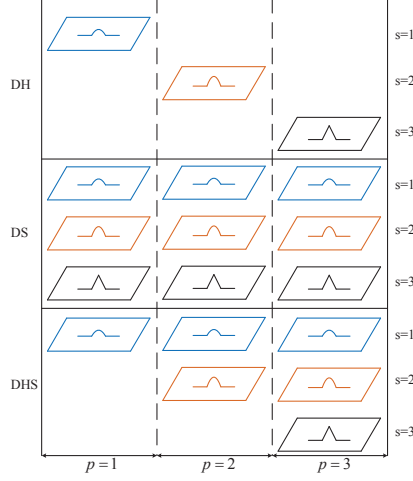
Figure 2.1. Multiresolution strategies of data: the most blurred, less blurred and original images are marked in blue, orange and black, respectively. p represents the resolution level of the registration process. The resolution level of data becomes finer with increasing scale s.

the transformation complexity:

$$\text{TH:} \qquad \mathbf{T}_{\boldsymbol{\mu}}^p(\mathbf{x}, s) = \mathbf{T}_{\boldsymbol{\mu}}^p(\mathbf{x}) = \mathbf{x} + \sum_{\mathbf{x}_i \in I_{\mathbf{x}}^p} \mathbf{c}_i^p \beta^r((\mathbf{x} - \mathbf{x}_i)/g(p)), \qquad (2.7)$$

$$\text{TS:} \qquad \mathbf{T}_{\boldsymbol{\mu}}^p(\mathbf{x}, s) = \mathbf{x} + \sum_{l=1}^s \sum_{\mathbf{x}_i \in I_{\mathbf{x}}^l} \mathbf{c}_i^l \beta^r((\mathbf{x} - \mathbf{x}_i)/g(l)), \qquad (2.8)$$

$$\text{THS:} \qquad \mathbf{T}_{\boldsymbol{\mu}}^p(\mathbf{x}, s) = \mathbf{x} + \sum_{l=1}^{\min(s,p)} \sum_{\mathbf{x}_i \in I_{\mathbf{x}}^l} \mathbf{c}_i^l \beta^r((\mathbf{x} - \mathbf{x}_i)/g(l)), \qquad (2.9)$$

where $\mathbf{T}_{\boldsymbol{\mu}}^p(\mathbf{x}, s)$ represents the transformation at registration level p for a given point $(\mathbf{x}, s)$ in the scale stack defined by (5.11). $l \in [1, S]$ denotes the B-spline grid level. $\mathbf{c}_i^p$ and $\mathbf{c}_i^l$ are the B-spline coefficient vectors at levels p and l, with corresponding grid spacings $g(p)$ and $g(l)$; the grid spacing $g(l)$ reduces with increasing l.

With TH, the transformation is upsampled after each resolution (i.e., $\mathbf{c}_i^p$ are determined based on $\mathbf{c}_i^{p-1}$ such that $\mathbf{T}_{\boldsymbol{\mu}}^p(\mathbf{x}, s) = \mathbf{T}_{\hat{\boldsymbol{\mu}}}^{p-1}(\mathbf{x}, s)$ at the start of level p) and only the currently finest level is being optimized, so $\boldsymbol{\mu}$ at level p consists of the elements of $\mathbf{c}_i^p$. In TS the transformation model is independent of registration level p. The whole transformation is a summation of multiple B-spline models with different grid spacings; the parameter vector $\boldsymbol{\mu}$ consists of all elements of $\mathbf{c}_i^l$, $\forall l \in [1, S]$. With THS, the transformation model is defined as a sum of multiple B-spline models; at resolution level p, the parameter vector $\boldsymbol{\mu}$ consists of all elements of $\mathbf{c}_i^l$, $\forall l \in [1, p]$. The THS model was called hierarchically simultaneous because it considers multiple B-spline control point resolutions simultaneously, but the finer B-spline models are only used in the later resolution levels. Figure 2.2 illustrates the TH, TS and THS
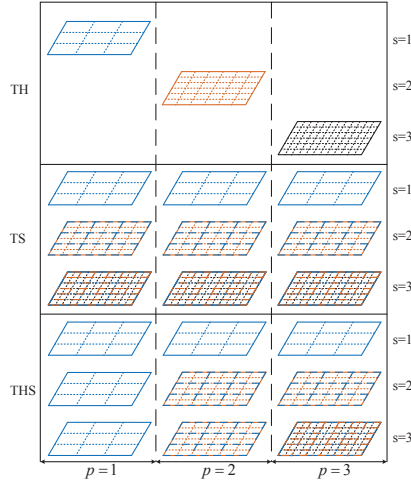
Figure 2.2. Multiresolution strategies of transformation: the coarsest, finer and finest B-spline grid are marked in blue, orange and black, respectively. The resolution level of transformation becomes finer with increasing scale s.

strategies, in the case of three resolution levels. In Figure 2.2, the coarsest, finer and finest B-spline grid are marked in blue, orange and black, respectively. In the TS row, for example, we can see that the coarsest, finer and finest transformation levels are used simultaneously in every registration phase p.

It should be noted that simultaneously using the B-spline basis functions of the different resolution levels leads to an overcomplete representation in the cases TS and THS. This could make the registration problem ill-posed, theoretically. The next subsection explains how we can still obtain a relatively well-posed optimization problem, thanks to selective coupling of transformation resolution levels and image resolution levels.

2.2.3   Combinations of Multiresolution Strategies

We can construct 3×3 combinations of multiresolution methods based on the three different multiresolution strategies for both data and transformation. Figure 2.3 shows all of these combinations when $S = 3$. The traditionally hierarchical multiresolution strategy is the combination of TH and DH. The coupling of transformation and image resolution levels is visualized by the combination of 'grids' and 'signal blobs' in the figure. Invalid combinations (to be discussed below) are marked by a red cross in the upper right corner.

Figure 2.3 demonstrates that the TH-DS method optimizes the current transformation level p using all data levels $[p, S]$. In a new registration level $p + 1$, the transformation will be initialized as: $\mathbf{T}_{\boldsymbol{\mu}}^{p+1}(\mathbf{x}, s) = \mathbf{T}_{\hat{\boldsymbol{\mu}}}^{p}(\mathbf{x}, s)$, and only one level of transformation works in one registration level. Differently, in TS-DS all levels of data and transformation are optimized simultaneously in every registration level. In

THS-DS, with its hierarchically simultaneous transformation model, the coarser transformation levels $[1, p-1]$ continue being optimized in later registration levels $[p, S]$, and the final transformation, which is applied to the finest resolution level of data, is the accumulative version of all resolution levels of transformation.

In Section 2.2.2 it was mentioned that the overcompleteness of the multi-level B-spline model used in TS and THS could lead to an ill-posed optimization problem. However, in combination with DS and DHS this problem is alleviated, by the coupling of each transformation resolution level with a different (set of) image resolution levels. For example, in TS-DS, the optimization problem is relatively well-posed, because the fine resolution transformation only affects the fine resolution image data, while the coarse resolution transformation affects both coarse and fine resolution levels of the image.

The problem is further alleviated by restricting that transformation level l (with the B-spline model with grid spacing $g(l)$) can only be applied to the finer image resolutions $s \in [l, S]$. Through this rule, the unexpected transformation by combining a finer grid spacing with a coarser resolution level of data will be eliminated. In Figure 2.3, these invalid combinations are marked with the red crosses in the upper right corners. As a result of this restriction, the combination of TH and DHS becomes equivalent to TH-DH. In addition, TS-DH and TS-DHS are equivalent to THS-DH and THS-DHS, respectively. To reflect this, we introduce the shorthand notation T(H)S-DHS to refer to the equivalent methods TS-DHS and THS-DHS, and similar notation for the other pairs of equivalent methods.

Only in the case T(H)S-DH, the problem remains ill-posed, since in the final registration stage $p = 3$, only fine resolution image data is taken into consideration, while all three transformation levels are being optimized simultaneously.

The combinations with DS and DHS strategies can be further distinguished by Sum and Union definitions which are introduced in Section 2.2.1. Therefore, we finally have the following 10 different multiresolution combinations: TH-DH, TH-DS (Sum and Union), TS-DH, TS-DS (Sum and Union), TS-DHS (Sum and Union), THS-DS (Sum and Union). Table 2.2 provides an overview of these combinations.

Table 2.2. Combinations of Multiresolution Strategies

	DH	DS	DHS
TH	a	b^*	a
TS	c	d^*	e^*
THS	c	f^*	e^*

The equivalent combinations are represented by the same alphabets, and the asterisk (*) indicates that Sum and Union definitions are possible.

2.3 Implementation details

The open source image registration package `elastix` [47] was used to implement our work. Similarity measures SSD and NCC were used as dissimilarity term $\mathcal{C}$ on lung
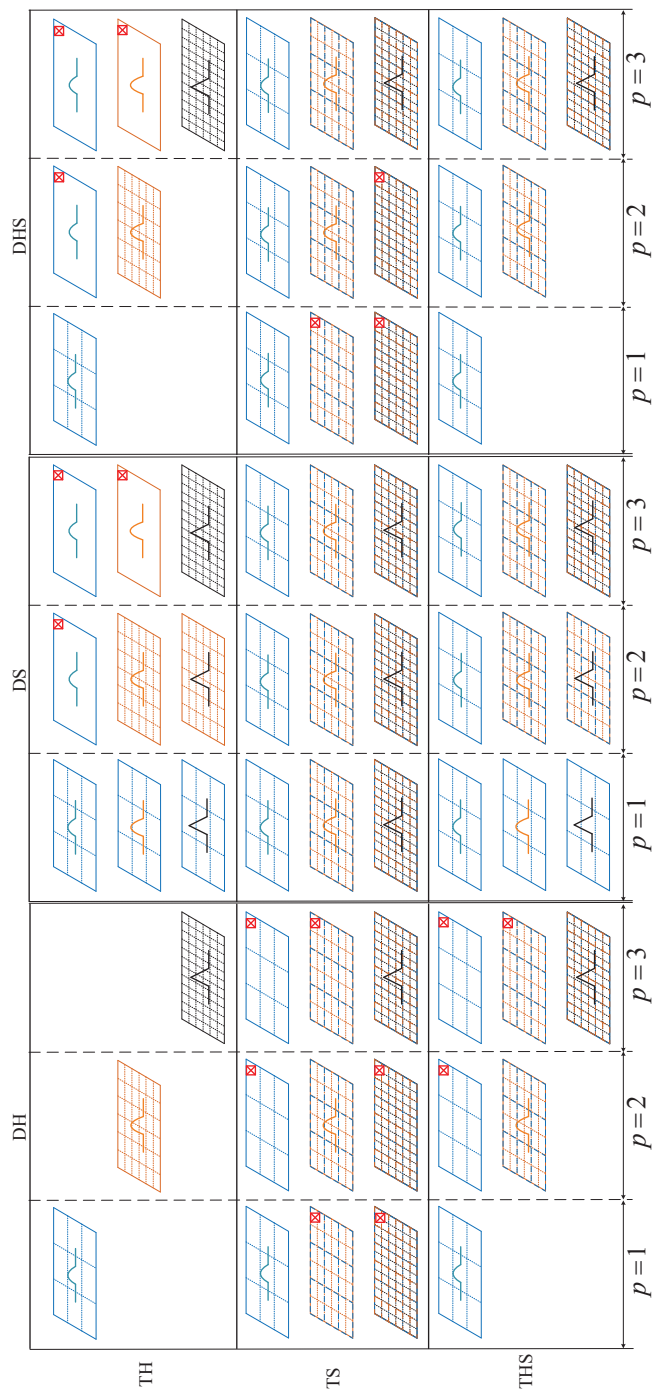
Figure 2.3. Different combinations of multiresolution strategies of data and transformation for multiresolution registration. Invalid combinations of resolution levels of data and transformation are marked with red crosses on their upper right corners.

and brain data, respectively. For the transformation model, a third order ($r = 3$) B-spline model was utilized. Trilinear interpolation was used to interpolate the moving image. We used the adaptive stochastic gradient descent optimizer (ASGD) [45] as optimization method, which uses only a small, randomly selected, subset of samples $(\mathbf{x}, s)$ from the entire image in each optimization iteration. To facilitate the joint optimization of the B-spline coefficients of different levels in TS and THS, a diagonal preconditioning matrix $\mathbf{B}$ was defined to scale the parameters corresponding to the different transformation levels:

$$\boldsymbol{\mu}_{k+1} = \boldsymbol{\mu}_k - \alpha_k \mathbf{B} \frac{\partial \mathcal{C}}{\partial \boldsymbol{\mu}}(\boldsymbol{\mu}_k), \tag{2.10}$$

where k is the current iteration number of optimization. $\boldsymbol{\mu}_{k+1}$ and $\boldsymbol{\mu}_k$ represent the new and current parameter vector, respectively, $\frac{\partial \mathcal{C}}{\partial \boldsymbol{\mu}}(\boldsymbol{\mu}_k)$ denotes the derivative of the cost function with respect to $\boldsymbol{\mu}$, α_k is a scalar gain factor that determines the step size [45], and $\mathbf{B}$ is a diagonal matrix $diag([b_{1,1}b_{1,1}b_{1,1} \ldots b_{l,l}b_{l,l}b_{l,l} \ldots b_{S,S}b_{S,S}b_{S,S}])$ with $b_{l,l} = \varepsilon^{-(S-l)}$. Based on initial trial-and-error experiments on 2D artificial images, we set $\varepsilon = 4$. The matrix $\mathbf{B}$ works as a preconditioning strategy [5], which can enhance the convergence rate of optimization. Intuitively, control points corresponding to coarse scales are updated less aggressively, because they affect a larger portion of the image, and thus have a larger effect on the cost function.

With ASGD as optimization method, the computational cost per iteration k is dominated by the cost of calculating $\frac{\partial \mathcal{C}}{\partial \boldsymbol{\mu}}$, which is linearly dependent on the number of samples used. Thus, if we choose the number of samples the same for each multiresolution method, the computational costs do not differ between DH, DS and DHS. The cost of transforming one sample, $\mathbf{T}_{\boldsymbol{\mu}}^p(\mathbf{x}, s)$, scales with s and $\min(s, p)$ in TS and TSH, respectively, compared with TH.

To investigate whether the differences in the performance of the multiresolution methods are due to our specific choice of optimization method, we performed a subset of experiments with a nonlinear conjugate gradient (NCG) [73] optimization method instead of the ASGD. In previous work [48] this state-of-the-art deterministic optimizer was shown to perform well in comparison with a wide range of other optimization methods. In [48] it was also found that stochastic gradient descent optimizers, such as ASGD, are more robust in the absence of a regularization term than conventional deterministic methods such as quasi-Newton and NCG. For fair comparison, experiments with NCG were therefore performed with a regularization term added to the cost function. As a regularization term, we chose the common bending energy (BE), as defined in [48]. The weighting value λ for the regularization term is an important parameter, and was tested in a wide range (see next section). Note that, since NCG is a deterministic optimization method, samples $(\mathbf{x}, s)$ are drawn once at the beginning of optimization, and not refreshed in every iteration. Naturally, the number of samples should be chosen considerably higher for NCG than for ASGD.

2.4   Experiments

In this section, the lung and brain imaging data are described first. Then, measures for registration accuracy and transformation smoothness are introduced in order to

evaluate the performances of different multiresolution combinations.

2.4.1 Lung data

DIR-Lab [15] provides 10 3D chest CT scans with 300 manually annotated landmarks in the lung structure. Table 3.1 provides a description of these data. Lung masks were created to limit the registration to the lung region [66]. The masks were created by thesholding, 3D-6-neighborhood connected component analysis, and morphological closing operation using a spherical kernel with a diameter of nine voxels.

Table 2.3. Description of DIR-Lab lung data.

Case No.	Dimensions	Voxelsize (mm)	Initial mTRE(mm)
1	$256 \times 256 \times 94$	$0.97 \times 0.97 \times 2.5$	3.89
2	$256 \times 256 \times 112$	$1.16 \times 1.16 \times 2.5$	4.34
3	$256 \times 256 \times 104$	$1.15 \times 1.15 \times 2.5$	6.94
4	$256 \times 256 \times 99$	$1.13 \times 1.13 \times 2.5$	9.83
5	$256 \times 256 \times 106$	$1.10 \times 1.10 \times 2.5$	7.48
6	$512 \times 512 \times 128$	$0.97 \times 0.97 \times 2.5$	10.89
7	$512 \times 512 \times 136$	$0.97 \times 0.97 \times 2.5$	11.03
8	$512 \times 512 \times 128$	$0.97 \times 0.97 \times 2.5$	14.99
9	$512 \times 512 \times 128$	$0.97 \times 0.97 \times 2.5$	7.92
10	$512 \times 512 \times 120$	$0.97 \times 0.97 \times 2.5$	7.30

For all cases, the exhale phase (moving image) is registered to the inhale phases (fixed image). In all test cases, $S = 4$ resolution levels were used. The image scale stacks were generated using $\{\sigma_1, \ldots, \sigma_S\} = \{4, 2, 1, 0.5\}$ voxels. In the experiments the finest grid spacing $g(S)$ was set to 8mm, 10mm, 13mm, or 16mm, and the coarsest grid spacing $g(1)$ was consistently set to 64mm, isotropically. Based on the changing $g(S)$ and fixed $g(1)$, the grid schedule for four transformation levels was calculated as $\{g(1), g(S)(g(1)/g(S))^{2/3}, g(S)(g(1)/g(S))^{1/3}, g(S)\}$. For example, the grid schedule for $g(s) = 8$mm is $\{64, 32, 16, 8\}$. For each optimization iteration, the number of random samples was set to 16000 for all combinations. Note that with the DS and DHS approaches these samples are spread over multiple levels of the image scale stack, whereas with DH all samples are placed in the current active level $s = p$. The number of iterations was set to 2000 per registration phase. Because the moving and fixed images are from the same patient, the intensity change between different breathing phases is limited. Therefore, SSD is used as the similarity metric to drive the registration. Since SSD is the similarity metric, the Sum and Union definitions, which are introduced in Section 2.2.1, become equivalent. Thus the registration results by the Sum and Union definitions are the same.

To evaluate the dependence on the optimization method, the experiments with CT lung data were repeated with the NCG optimizer. In this case, we used 100000 samples, and limited the number of iterations to 100 per registration phase. Through initial trial-and-error experiments, the optimum value of the weighting value λ for the BE regularization term was estimated to be around $10^5 - 10^7$, depending on the

setting of $g(S)$ and the particular multiresolution strategy. Therefore, we tested all methods for a range of $\lambda \in \{10^3, 10^4, \ldots, 10^9\}$.

2.4.2   Brain data

The Internet Brain Segmentation Repository (IBSR v2.0) contains 18 T1-weighted MRI 3D brain scans, which were also used to evaluate our multiresolution strategies. These brain scans have been positionally transformed into Talairach space [102] and have been processed by the CMA (Center for Morphometric Analysis) bias field correction routines [44]. The volumes of these images are $256 \times 256 \times 128$mm. The voxel sizes are divided into three groups (8: $0.94 \times 0.94 \times 1.5$, 6: $0.84 \times 0.84 \times 1.5$, 4: $1 \times 1 \times 1.5$).

To evaluate the performance of different multiresolution strategies, intersubject registration was carried out on these data, which resulted in 18×17 test cases. As in the lung experiment, $S = 4$ resolution levels were used. The image scale stacks were generated using $\{\sigma_1, \ldots, \sigma_S\} = \{4, 2, 1, 0.5\}$ voxels as well. Different from the lung experiments, the finest grid spacing $g(S)$ was set to 8mm and 5mm, isotropically, and the grid schedule for four transformation levels was calculated as $\{8 \times g(S), 4 \times g(S), 2 \times g(S), g(S)\}$. For brain data, these are common settings. For each optimization iteration, the number of random samples was set to 16000 for all combinations as in the lung experiments, and the number of iterations was also set to 2000 per registration phase. Since global intensity differences between moving and fixed data may be present, NCC, which can handle linear intensity changes, was used as the similarity metric to drive the registration. As described in Section 2.2.1, the Sum and Union definitions will produce different cost functions when NCC is used. Therefore, the registration results from different definitions could be different. Because these data sets were acquired at different laboratories, and the ages of patients range from 7 to 71, the anatomical difference could be large between patients. Therefore, initial affine registration was used to roughly align the data first, and then these initialized results were utilized as the input data for the nonrigid registration experiments with different multiresolution strategies.

2.4.3   Evaluation measures

In our evaluation, both registration accuracy and transformation smoothness were considered. The mean of target registration error (mTRE) and segmentation overlap were utilized to compare the registration accuracy of multiresolution registration methods. Moreover, the determinant of the spatial Jacobian D_{SJ} was used to evaluate the smoothness of the spatial Jacobian of the deformation.

2.4.3.1   mTRE

Since 300 manually marked landmarks were provided with the lung data, mTRE [115] can be used to evaluate the registration accuracy:

$$\text{mTRE} = \frac{1}{n} \sum_{i=1}^{n} \| \mathbf{T}_{\hat{\boldsymbol{\mu}}}(\mathbf{p}_i^F) - \mathbf{p}_i^M \|, \tag{2.11}$$

where $\mathbf{p}_i^F$ and $\mathbf{p}_i^M$ represent the corresponding ground truth landmarks in fixed and moving images, respectively. $n = 300$ is the number of landmarks in all test cases.

2.4.3.2 Overlap

In the brain data, 84 manually labeled regions are available. With these labels we can use mean overlap (MO) [44] to measure the registration accuracy:

$$\text{Mean Overlap} = 2 \frac{\sum_r |M_r \cap F_r|}{\sum_r (|M_r| + |F_r|)}, \tag{2.12}$$

where r represents a certain label, and the MO is calculated over all labels.

2.4.3.3 Smoothness of deformation field

Besides the registration accuracy, the smoothness of transformation is an important measure to evaluate the performance of a registration method. In this work, D_{SJ} is used to measure the smoothness of the transformation. For a given spatial location $\tilde{\boldsymbol{x}}$, D_{SJ} can be calculated as:

$$D_{SJ} = \left| \frac{\partial \mathbf{T}_{\boldsymbol{\mu}}}{\partial \boldsymbol{x}}(\tilde{\boldsymbol{x}}) \right|. \tag{2.13}$$

If $D_{SJ} > 1$, the deformation around $\tilde{\boldsymbol{x}}$ is a local expansion. A local contraction happens when $0 < D_{SJ} < 1$. If D_{SJ} is negative, a folding region exists at that location. In a folding region, the topological consistency is not preserved. In a smooth transformation field, the fluctuation of D_{SJ} will be relatively small. Therefore, we utilized the standard deviation of D_{SJ} to represent the smoothness of the deformation field.

2.5 Results

In this section, we present the results of the different multiresolution methods on both lung and brain data.

2.5.1 Lung data

Figure 2.4 shows the registration results of all multiresolution combinations on the lung data using the ASGD optimizer. As described in Section 2.2.3, TH-DHS, TS-DH and TS-DHS are actually equivalent to TH-DH, THS-DH and THS-DHS, respectively. So the results of TH-DH, THS-DH and THS-DHS were assigned to their equivalent combinations. Herewith, we facilitate the comparison among different multiresolution strategies of data and transformation in a general view. From Figure 2.4, it can be observed that the traditional TH-DH approach has relatively worse performance than TH-DS and THS-DS in most cases. Especially in test cases c4, c6 and c8-9, TH-DH yields unsatisfactory results. In c4, c6-7, and c9, the registration accuracy of TH-DH deteriorates rapidly with decreasing grid spacing of the B-spline model. In addition, the results by TS-DS are unstable when compared to the relatively consistent

performance of TH-DS and THS-DS. Heinrich *et al.* [34] used a similar experimental setting and the same lung data as in this study. If we compare the best results in both researches, the simultaneous registration methods produced more accurate results on 7 lung cases. In the chapter by Metz *et al.* [66], the first five cases were also used in the evaluation of their registration method. Compared with their results, our results are comparable.

A box plot of the mTRE values using the ASGD optimizer for each multiresolution method on different test cases is shown in Figure 2.5 (a). For each method, the corresponding box plot covers all 4 different $g(S)$. It can be seen that TH-DS and THS-DS generate better registration accuracy than the other methods over all test cases, especially looking at the upper quartile and the number of outliers. The upper quartiles of mTRE produced by TH-DS, THS-DS, and TH-DH are 1.46mm, 1.47mm and 2.05mm, respectively.

Figure 2.5 (b) shows a box plot of the standard deviation of D_{SJ} for each multiresolution method on different test cases using the ASGD optimizer. We can find that THS-DS generates the smoothest transformations over all test cases. To visualize the properties of the resulting transformation field, a color-encoded visualization method was used in Figure 2.6. For each voxel on the selected slice, the corresponding D_{SJ} value was calculated. In Figure 2.6 the dark blue and red colors indicate least smooth local contraction and expansion, respectively. This example shows that THS-DS produces the smoothest transformation field. The other multiresolution combinations result in less smooth transformation fields, and TS-DS generates the most extreme transformation field.

To make a further comparison among the different multiresolution combinations, a two dimensional ranking of the 9 methods using the ASGD optimizer was made for each test case. 10×4 test cases are generated by 10 lung data pairs with 4 different final grid spacings. The average rank of each method over all 10×4 test cases is presented in Figure 2.7. In Figure 2.7 the X-axis indicates the ranking in registration accuracy, and the Y-axis represents the ranking in smoothness. Here, the lower ranking number means better performance. We can see that THS-DS has a relatively better registration accuracy and smoothness than the other combinations. Although the registration accuracy of TH-DS is a little better than THS-DS, its smoothness only reaches the fifth ranking number among all 9 methods. Compared to the other multiresolution combinations, TS-DS and traditional TH-DH(S) approaches have relatively worse average ranking numbers in both registration accuracy and smoothness. TS-DH and its equivalent THS-DH perform still better than TH-DH(S) and TS-DS, but not as good as the combination THS-DS.

Figure 2.5 (c) shows a box plot of the mTRE values for all multiresolution methods using the NCG optimizer and the BE regularization term. For each method, the corresponding box plot covers 4 different $g(S)$ and 7 different λ values. Figure 2.5 (d) shows the box plots of the standard deviation of D_{SJ}. Similar as with ASGD, TH-DS and THS-DS generate better registration accuracy (especially less outliers) than the other methods, and THS-DS generates the smoothest transformations over all test cases. Please note that the scales of the vertical axes are different, because the NCG method with low regularization weight resulted in higher registration errors. Also in previous work [48] it was found that stochastic gradient descent optimizers, such as

Figure 2.4. Performance comparison of different multiresolution combinations using ASGD optimizer on the ten lung cases. The numbers represent the mTRE in millimeters.

Figure 2.5. Performances of accuracy and smoothness by all multiresolution methods on lung data. An asterisk (*) behind the label indicates the result is significantly different (paired Wilcoxon signed rank test, $p < 0.05$) from TH-DH(S): (a) mTRE by ASGD optimizer. Each box plot represents the mTRE values by each multiresolution method on 10 patients using 4 different $g(S)$; (b) standard deviation of D_{SJ} using ASGD optimizer. Each box plot represents the standard deviation of D_{SJ} by each multiresolution method on 10 patients using 4 different $g(S)$; (c) mTRE of all multiresolution methods using NCG optimizer and BE term. Each box plot represents the mTRE values by each multiresolution method on 10 patients using 4 different $g(S)$ and 7 different λ; (d) standard deviation of D_{SJ} using NCG optimizer and BE term. Each box plot represents the standard deviation of D_{SJ} by each multiresolution method on 10 patients using 4 different $g(S)$ and 7 different λ.

ASGD, are more robust in the absence of a regularization term than conventional deterministic methods such as quasi-Newton and NCG. For the highest weight of the regularization term, all multiresolution strategies converged to an almost identical result, with relatively low accuracy, since any local nonrigid deformations are penalized heavily.

Paired Wilcoxon signed rank tests [37] were performed to verify the statistical significance of the registration results on lung data. The paired comparisons were carried out between the TH-DH method and the other methods on registration accuracy and smoothness. In Figure 2.5, the methods that produced significantly different ($p < 0.05$) results from TH(S)-DH are marked by asterisks.

To investigate in more detail in which cases the various methods lead to different results, we plotted initial registration accuracy (before nonrigid registration) versus final registration accuracy (after nonrigid registration), inspired by the robustness
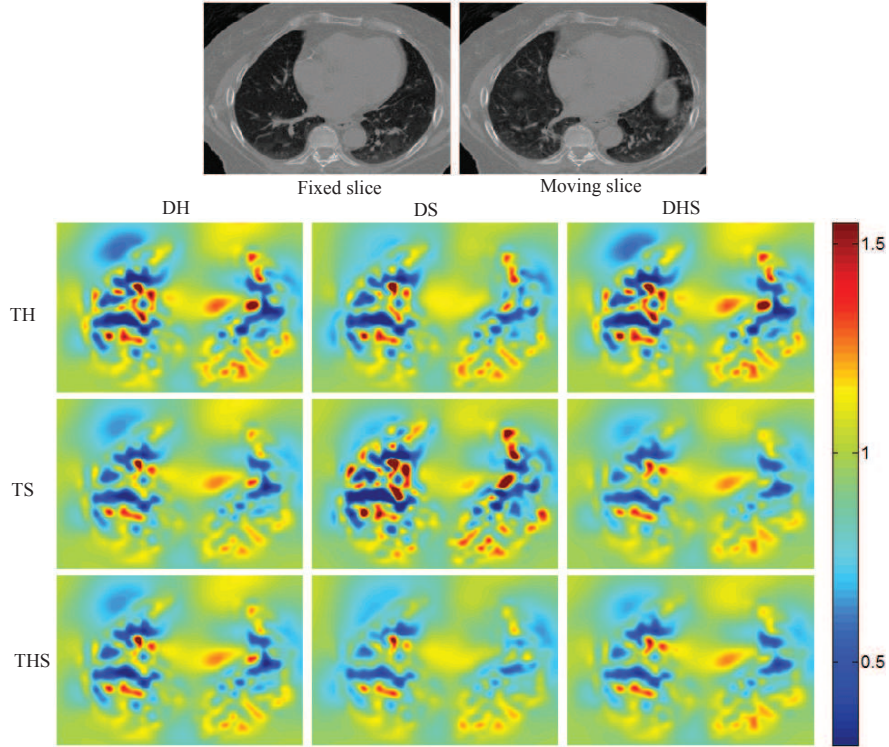
Figure 2.6. An example D_{SJ} map of the transformation fields by different multiresolution strategies on lung data from c9 using ASGD optimizer.

plots in [108]. Figure 2.8 (a) and (b) show the robustness analysis based on the registration results by ASGD optimizer, and NCG optimizer with BE regularization term, respectively. The X-axes of Figure 2.8 represent the initial Euclidean distance (IED) for each pair of corresponding landmarks, binned for every 5mm for a clearer display. The Y-axes of Figure 2.8 show the registered Euclidean distance (RED) for each pair of corresponding landmarks. Within each bin, the IED values and the resulting RED values were averaged for each registration method. Figure 2.8 (a) and (b) demonstrate that there is no clear correlation between the initial misregistration and the resulting registration error for TH-DS and THS-DS. In Figure 2.8 (a), the robustness of TH-DS and THS-DS are consistently good for various IEDs. However, we can find that TS-DS, TH-DH(S), T(H)S-DH, and T(H)S-DHS become relatively unstable for some landmark pairs with which are initially far away (i.e. have a high IED). It can be found that the TS-DS method suffers most from this problem. Figure 2.8 (b) confirms these results for the NCG optimizer with BE regularization.
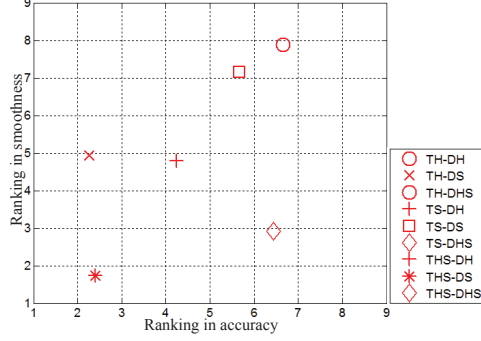
Figure 2.7. Two dimensional averaged ranking number of the 9 multiresolution methods in 40 test cases using the ASGD optimizer.
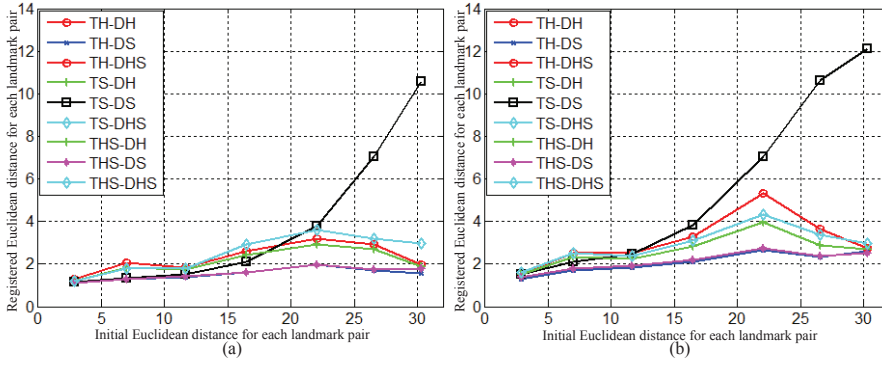
Figure 2.8. Robustness analysis, plotting Euclidean distance (in mm) between corresponding landmarks before and after nonrigid registration for: (a) registration using the ASGD optimizer; (b) registration using the NCG optimizer and BE regularization term with $\lambda \in \{10^3, \ldots, 10^9\}$.

2.5.2   Brain data

Figure 2.9 shows the box plot of 18×17 MO values of different multiresolution methods with finest grid spacing $g(S)$ of 8mm and 5mm. We can see that the registration accuracy of all methods is improved after $g(S)$ was decreased to 5mm. Different from the results in the lung experiments, TS-DS produced the best registration accuracy on the brain data. Similar to the results in the lung experiments, TH-DS and THS-DS obtained consistently better registration accuracy than the other multiresolution methods except TS-DS. From Figure 2.9 we can also notice that the Sum and Union definitions gave similar results.

The IBSR data in this study have been used in [44] as well. Although the experimental settings and accuracy measures are different between the two studies, the registration accuracy presented in this work is comparable with the accuracy reported in [44].

The smoothness of the transformation is compared in Figure 2.10, which shows box plots of the standard deviation of D_{SJ}. It can been seen that THS-DS produces the smoothest transformation. While giving the highest registration accuracy, the smoothness of TS-DS performs much worse. In Figure 2.10 we can also notice that THS produces smoother results than TH and TS.

As on lung data, we performed paired Wilcoxon signed rank tests for determining the statistical significance of the registration results on brain data. The paired comparisons were carried out between the TH-DH method and the other methods on registration accuracy and smoothness. In Figures 9 and 10, the methods that produced significantly different ($p < 0.05$) results from TH-DH are marked by asterisks.

A two dimensional ranking of the 14 multiresolution methods was made to further compare these combinations for each $g(S)$. In Figure 2.11, the X-axis represents the ranking in registration accuracy, and the Y-axis indicates the ranking in smoothness. As in Figure 2.7, a lower ranking number means better performance. We can see that the Sum and Union definitions of TS-DS produce the best ranking in registration accuracy. However, the smoothness of TS-DS is unsatisfactory. If both registration accuracy and smoothness are considered as the criterion to measure registration performance, THS-DS has a relatively better performance than the other methods in Figure 2.11(b). Although the registration accuracy of TH-DS is a little better than THS-DS, its smoothness is almost the worst among the 14 multiresolution methods. Compared to the other multiresolution methods, the TH-DH(S) approach produces relatively worse average ranking numbers in both registration accuracy and smoothness. TS-DH and its equivalent THS-DH perform slightly better than TH-DH(S), but still have a relatively high ranking number for smoothness, compared with THS-DS.

To investigate the relation between the overlap of each brain structure before nonrigid registration and after nonrigid registration, a robustness analysis was performed for each $g(S)$. The X-axes of Figure 2.12 (a) and (b) represent the initial overlap (IO) value for each brain structure before the nonrigid registration, binned into bins of 0.05 for clearer display. The Y-axes of Figure 2.12 (a) and (b) represent the registered overlap (RO) value after the nonrigid registration for each corresponding brain label. Within each bin, the IO values and the corresponding RO values were averaged for each registration method. The figure shows that the largest differences in registration accuracy between multiresolution methods are observed for structures with relatively low initial overlap. Again, the differences between methods are more pronounced for $g(S) = 5mm$ than for $g(S) = 8mm$.

2.6   Discussion

Multiple multiresolution strategies for both the data and the transformation model in FFD image registration were defined and evaluated in this work. In two applications, we found that DS usually generates better registration accuracy than DH and DHS. Compared to the traditionally hierarchical multiresolution strategy DH, simultaneous multiresolution registration has the ability to consider the coarser and finer resolutions simultaneously, so that global and local information can be combined to avoid local minima. In this way, more accurate and robust registrations are ob-

tained. For the multiresolution strategy of the transformation, THS often produced smoother transformations than TH and TS. In the traditionally hierarchical multiresolution strategy of transformation, the finer transformation level is initialized with the coarser transformation level, and only one level of transformation is being optimized at once. In the THS strategy, the coarser transformation levels continue being optimized, which apparently has a regularizing effect on the optimization. Similar to our former work [98], Shi *et al.* [90] have proven that a multi-level FFD can recover the discontinuous motion better than the traditionally hierarchical FFD.

The registration accuracy of TS-DS on the brain data is quite different from the results on the lung data. In the TS-DS method, the fine-resolution data and transformation levels are active from the start of registration. This creates a chance for a large deformation to be captured by a finer transformation level rather than a more suitable coarser transformation level. The consistently higher standard deviation of D_{SJ} produced by TS-DS confirms that this likely leads to less smooth deformation fields. The small vessels in the lung scans can be influenced by this unsmooth transformation field, which is reflected by the higher mTRE values for the anatomical landmarks that are used to measure the registration accuracy. Rohlfing [83] has shown that overlap scores can still be very high even for some discontinuous transformation fields. Although the IBSR brain segmentations consist of 84 relatively small regions, this might still not be sufficiently detailed to detect the irregularities in the deformation field.

As shown in the results of registration accuracy for the lung data, the TH-DH(S) and TS-DS methods are sensitive to the spacing of B-spline control points. In many cases, the results by TH-DH and TS-DS deteriorate rapidly with a decrease in $g(S)$. Compared to TH-DH and TS-DS, TH-DS and THS-DS are more robust to the change of grid spacing.

Except for the registration accuracy by TS-DS, the experiments on the brain data confirm the results on the lung data. Since NCC is used as similarity metric, the Sum and Union definitions result in different registration methods. In Figure 2.9, the Union definition generated slightly better results than the Sum definition, but the differences are very small. THS-DS still produces the smoothest transformations on brain data.

The robustness analyses on both lung and brain data indicate that most differences between multiresolution methods are observed for structures with a relatively large initial misalignment.

Experiments on lung data with an alternative optimization method (NCG) showed similar relative differences in performance between the various multiresolution methods. These consistent results suggest that the better performances of simultaneous methods are relatively independent from the selection of optimizer.

If registration methods have similar registration accuracy, the one which results in a smoother transformation would be more attractive. To obtain a smoother transformation, a regularization term is often added to the cost function to obtain a smoother and more plausible transformation. Because the optimal weighting value of the regularization term could change for different image data or even different regions in a certain image, determining the weighting factor of the regularization term is a challenging problem. There is much literature [58, 76, 81] which discusses how to choose this weighting value. However, it might be more preferable to obtain regularized

results without regularization term. In all our experiments, THS-DS generates the smoothest transformation field with competitive accuracy among the multiresolution strategies. With different patients and different $g(S)$, the results of THS-DS are consistently smoother than other combinations. THS-DS continues optimizing the coarse transformation level in all registration phases, and the final transformation is the sum of different resolution levels of B-spline grids. In this way, large deformations are expected to be recovered and represented by the coarse transformation level. Then, the remaining detailed deformation can be captured by subsequent finer transformation levels.

As introduced in Section 2.3, we fixed ε to 4 in all experiments, which was based on initial tests on 2D artificial images. This value may not be optimal for 3D images as the affected volume per B-spline control point changes by a factor of 8 between adjacent scales. Also the use of a regularization may change the optimal value of ε. In future work, it could be interesting to derive a data-driven method for setting ε. Furthermore, as this study demonstrates the potential of using simultaneous multiresolution strategies, this opens the door for future research on deriving more advanced combination strategies, optimally combining the information from multiple scales.

2.7 Conclusion

In this chapter, different multiresolution strategies for data and transformation model in nonrigid registration were presented and compared. CT lung and T1-weighted MRI brain data were used to evaluate the multiresolution strategies in terms of accuracy and deformation smoothness. The multiresolution methods using a simultaneous data (DS) strategy had better registration accuracy than hierarchical (DH) and hierarchically simultaneous data (DHS) strategies. For the smoothness of the transformation field, the hierarchically simultaneous transformation (THS) strategy produced smoother transformation than the hierarchical (TH) and simultaneous strategies (TS). Summarizing, a simultaneous multiresolution strategy of data can enhance the registration accuracy, and a hierarchically simultaneous transformation strategy leads to smoother transformations. Analyses of robustness indicated that most differences between multiresolution methods were observed for structures with a relatively large initial misalignment, which corresponds to intuition. Considering different applications, registration accuracy and smoothness may have different importance. Therefore, we cannot conclude which combination is to be preferred in general. However, for both registration accuracy and smooth transformation, the method with hierarchically simultaneous transformation and simultaneous data strategies (THS-DS) is a better choice than the traditionally hierarchical strategy. All of the multiresolution combinations discussed in this work will be available as part of the open source registration package `elastix` for public application.
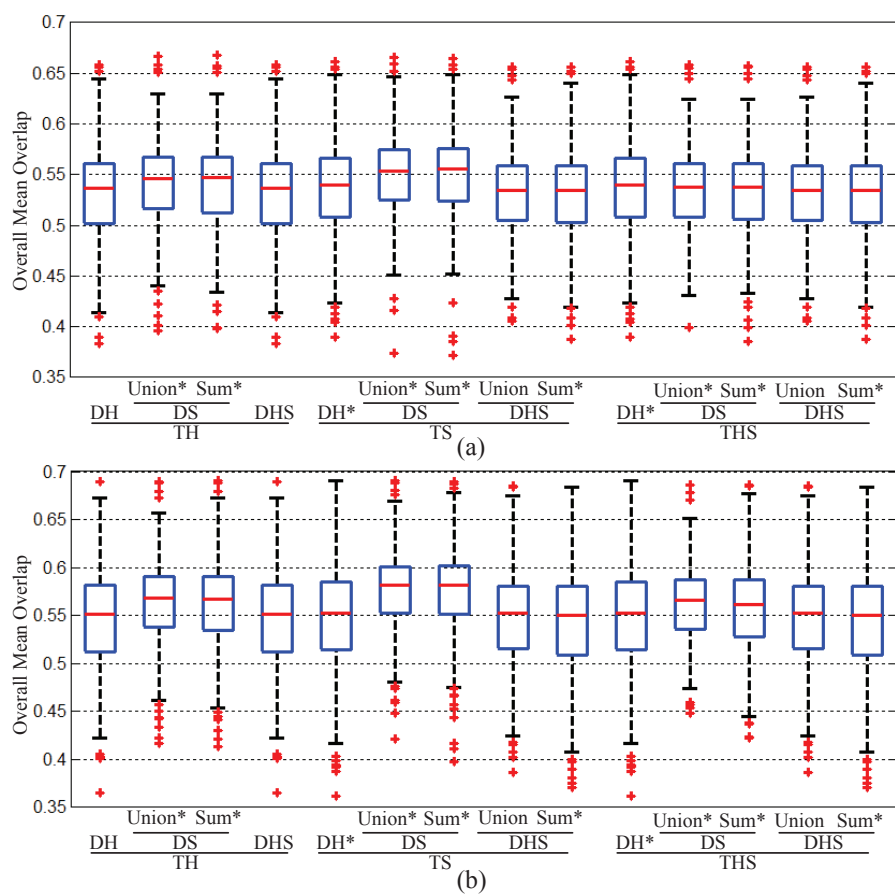
Figure 2.9. Performance comparison of different multiresolution methods using overall mean overlap: (a) $g(S) = 8mm$; (b) $g(S) = 5mm$. An asterisk (*) behind the method label indicates the result is significantly different (paired Wilcoxon signed rank test, $p < 0.05$) from TH-DH(S).
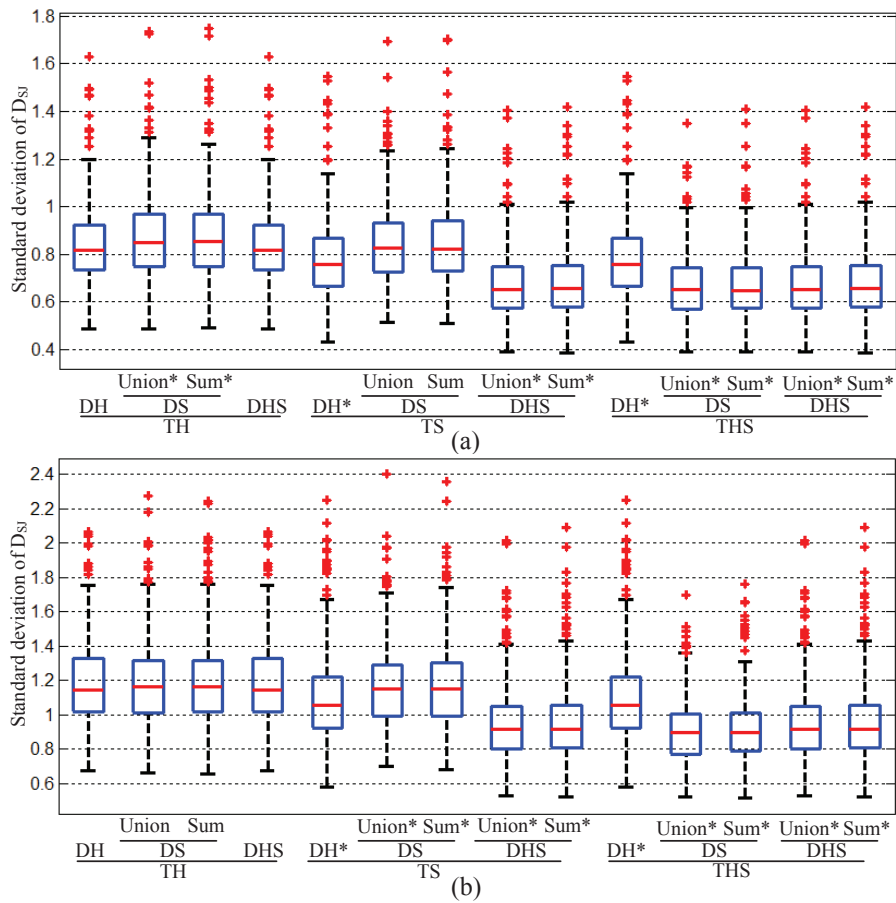
Figure 2.10. Standard deviation of D_{SJ} in 306 test cases: (a) $g(S) = 8mm$; (b) $g(S) = 5mm$. An asterisk (*) behind the method label indicates the result is significantly different (paired Wilcoxon signed rank test, $p < 0.05$) from TH-DH(S).
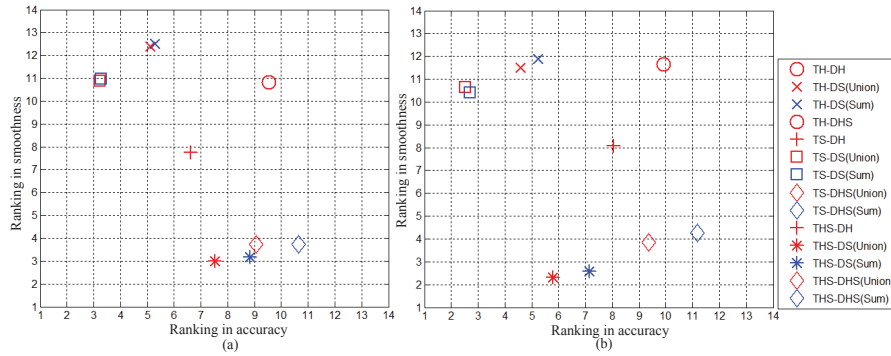
Figure 2.11. Two dimensional averaged ranking number of the 14 multiresolution methods in 306 test cases: (a) $g(S) = 8mm$; (b) $g(S) = 5mm$.
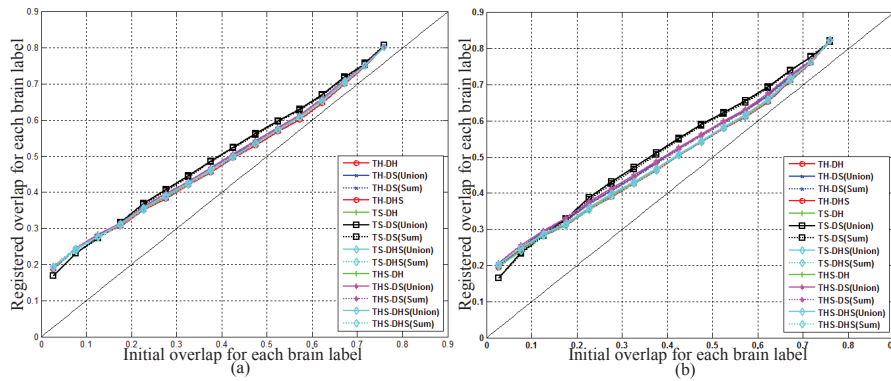
Figure 2.12. Robustness analysis, plotting initial overlap (before nonrigid registration) versus registered overlap (after nonrigid registration) of individual brain structures, for (a) registration with $g(S) = 8mm$; (b) registration with $g(S) = 5mm$.

Wavelet based free-form deformations for nonrigid registration

Abstract — In nonrigid registration, deformations may take place on the coarse and fine scales. For the conventional B-splines based free-form deformation (FFD) registration, these coarse- and fine-scale deformations are all represented by basis functions of a single scale. Meanwhile, wavelets have been proposed as a signal representation suitable for multi-scale problems. Wavelet analysis leads to a unique decomposition of a signal into its coarse- and fine-scale components. Potentially, this could therefore be useful for image registration. In this work, we investigate whether a wavelet-based FFD model has advantages for nonrigid image registration. We use a B-splines based wavelet, as defined by Cai and Wang [13]. This wavelet is expressed as a linear combination of B-spline basis functions. Derived from the original B-spline function, this wavelet is smooth, differentiable, and compactly supported. The basis functions of this wavelet are orthogonal across scales in Sobolev space. This wavelet was previously used for registration in computer vision, in 2D optical flow problems [119], but it was not compared with the conventional B-spline FFD in medical image registration problems. An advantage of choosing this B-splines based wavelet model is that the space of allowable deformation is exactly equivalent to that of the traditional B-spline. The wavelet transformation is essentially a (linear) reparameterization of the B-spline transformation model. Experiments on 10 CT lung and 18 T1-weighted MRI brain datasets show that wavelet based registration leads to smoother deformation fields than traditional B-splines based registration, while achieving better accuracy.

3.1   Introduction

T he classical B-splines based FFD registration [85] is a popular method for nonrigid medical registration. Compared with other registration approaches, B-spline FFD produces competitive results in different applications. In most implementations, a hierarchical strategy is used, in which the detailed (small scale) deformations are gradually estimated and added to the previously estimated global (large scale) deformations. The large and small deformations are mixed together in one B-spline transformation level, since they are all represented by B-spline basis functions with a uniform grid spacing.

For a multi-scale signal, wavelet analysis has been proposed to decompose the signal into different scales in a unique way. The wavelet decomposition could therefore be useful in nonrigid registration. Since there are numerous wavelet models proposed in the past, a suitable choice of desirable wavelet has to be made. As a nonrigid transformation model, the wavelet should be differentiable, compactly supported and orthogonal between different scales. Cai and Wang [13] proposed a B-splines based wavelet model which fulfills our requirements in Sobolev space. This wavelet model was previously used for 2D optical flow problems in computer vision [119]. The Cai-Wang wavelet model is a linear combination of three cubic B-spline basis functions. Therefore, a fair comparison is possible between this wavelet and the original B-splines based FFD registration. The aim of this work is to investigate whether a wavelet-based FFD model has advantages for nonrigid medical image registration.

(a)   (b)
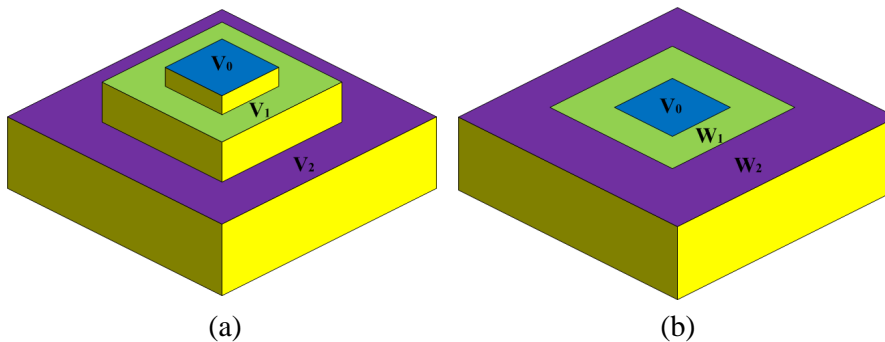
Figure 3.1. Redundant B-spline and non-redundant wavelet representations: (a) B-spline; (b) wavelet.

3.2   Method

3.2.1   Background on B-spline wavelet

The FFD model is usually constructed based on the cubic B-splines $\phi(x)$ [85]. Figure 4.1 (a) shows the curve of $\phi(x)$ in the one-dimensional case. For any $s, k \in \mathbb{Z}$ and

$0 \le s \le S$, we can define the scaling and translation of $\phi(x)$ as

$$\phi_{s,k}(x) = \phi(x/g_s - k), \tag{3.1}$$

where s represents the resolution level of one B-splines based FFD transformation level, and k represents the control points on a regular grid. The grid spacing $g_s = 2^{S-s}g_S$ becomes finer as s increases, and g_S is the finest spacing which is usually chosen by the user.

Let I denote a finite interval, i.e., $I = [0, L]$, where $L \in \mathbb{Z}^+$. Then the Sobolev space $H^2(I)$ which contains all continuous functions $f(x)$ with finite energy norm up to the second derivative can be described as

$$H^2(I) = \{f(x) \mid x \in I, \|f^{(i)}\|_2 < \infty, i = 0, 1, 2\}, \tag{3.2}$$

where $H^2(I)$ is also a Hilbert space with the inner product

$$\langle f, g \rangle = \int_I f''(x)g''(x)dx, \tag{3.3}$$

thus, $\|f\| = \langle f, f \rangle^{(1/2)}$ provides a norm for $H^2(I)$. For each resolution level s, $\{\phi_{s,k}(x) \mid 0 \le k \le L/g_s\}$, spans a closure V_s using norm $\|\cdot\|$. In previous research [13], it has been proven that V_s forms a multiresolution analysis (MRA) for $H^2(I)$,

$$V_0 \subset V_1 \subset \ldots \subset V_S \subset \ldots \subset H^2(I). \tag{3.4}$$

Equation (3.4) shows that the conventional B-spline basis function has the ability to represent a function in $H^2(I)$ in an MRA way.

To construct a wavelet decomposition of $H^2(I)$, Cai and Wang [13] presented a wavelet function $\psi(x)$ corresponding to $\phi(x)$,

$$\psi(x) = -\frac{3}{7}\phi(2x) + \frac{12}{7}\phi(2x-1) - \frac{3}{7}\phi(2x-2), \tag{3.5}$$

where $\psi(x)$ is orthogonal to $\phi(x)$ in $H^2(I)$, and $\phi(x)$ serves as the so-called "scale" function corresponding to the wavelet function $\psi(x)$. Figure 4.1 (b) plots the curve of $\psi(x)$, showing that $\psi(x)$ is symmetrical and compactly supported. Similar to $\phi(x)$, $\{\psi_{s,k}(x) = \psi(x/g_s - k) \mid 0 \le k \le L/g_s\}$ spans a closure W_s. It has been proven that W_s is the orthogonal complement of V_s in V_{s+1} under the inner product (3.3) (i.e., $V_{s+1} = V_s \oplus W_s$) and $H^2(I) = V_0 \oplus_{s \in \mathbb{Z}^+} W_s$.

Based on the wavelet decomposition, any one-dimensional function $f(x) \in H^2(I)$ can be approximated as closely as needed by a function $f_S(x) \in V_S = V_0 \oplus W_0 \oplus W_1 \oplus \cdots \oplus W_{S-1}$ for a sufficiently large S, and $f_S(x)$ has a unique orthogonal decomposition using basis functions $\phi_0(x)$ and $\{\psi_{s,k}(x) \mid 0 \le k \le L/g_s, 0 \le s \le S-1\}$.

Since higher dimensional data rather than one-dimensional data are used in medical registration, the tensor product is used to extend the one-dimensional wavelet approximation to two, three or even higher dimensions.
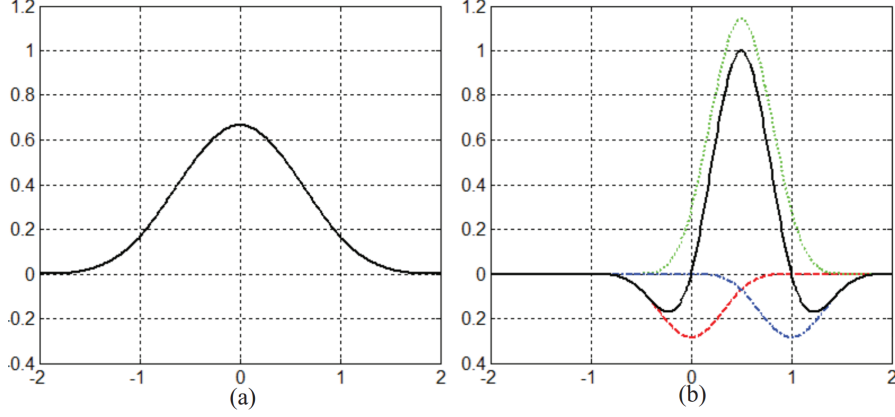
Figure 3.2. One-dimensional cubic B-spline function and its corresponding wavelet function: (a) $\phi(x)$; (b) $\psi(x)$ marked in black, and its three components are (red: $-\frac{3}{7}\phi(2x)$, green: $\frac{12}{7}\phi(2x-1)$, blue: $-\frac{3}{7}\phi(2x-2)$).

3.2.2 Application to image registration

In this section, we provide the two different definitions of the FFD transformation model: 1) using B-splines, and 2) using wavelets. For a 3D registration, let $\Phi(\mathbf{x})$: $\mathbb{R}^3 \to \mathbb{R}$ denote the three-dimensional tensor product of (3.1), $\phi(x_1)\phi(x_2)\phi(x_3)$ where $\mathbf{x} = (x_1, x_2, x_3)$, and $\Phi_{s,\boldsymbol{\xi}}(\mathbf{x}) = \Phi(\mathbf{x}/g_s - \boldsymbol{\xi})$ where $\boldsymbol{\xi}$ represent control points on a 3D grid. Then, the B-splines based FFD can be defined as follows

$$\mathbf{T}_{\boldsymbol{\mu}}^{S}(\mathbf{x}) = \mathbf{x} + \sum_{\boldsymbol{\xi} \in \mathbb{Z}^3} \mathbf{c}_{S,\boldsymbol{\xi}} \Phi_{S,\boldsymbol{\xi}}(\mathbf{x}), \tag{3.6}$$

where $\mathbf{c}$ are the coefficient vectors for control points $\boldsymbol{\xi}$, and the parameter vector $\boldsymbol{\mu}$ is formed by the elements of all coefficient vectors ($\boldsymbol{\mu} = \{\mathbf{c}_{S,\boldsymbol{\xi}} \mid \boldsymbol{\xi} \in \mathbb{Z}^3\}$).

Let $\boldsymbol{\Psi}(\mathbf{x}) : \mathbb{R}^3 \to \mathbb{R}^7$ denote a vector function which consists of seven different three-dimensional tensor products of scale and wavelet basis functions on a given resolution level,

$$\begin{aligned}
\boldsymbol{\Psi}(\mathbf{x}) \quad = \quad & [\phi(x_1)\phi(x_2)\psi(x_3), \\
& \phi(x_1)\psi(x_2)\phi(x_3), \\
& \psi(x_1)\phi(x_2)\phi(x_3), \\
& \psi(x_1)\psi(x_2)\phi(x_3), \\
& \psi(x_1)\phi(x_2)\psi(x_3), \\
& \phi(x_1)\psi(x_2)\psi(x_3), \\
& \psi(x_1)\psi(x_2)\psi(x_3)].
\end{aligned} \tag{3.7}$$

Then, the wavelet FFD is defined as

$$\mathbf{T}_{\boldsymbol{\nu}}^{S}(\mathbf{x}) = \mathbf{x} + \sum_{\boldsymbol{\xi} \in \mathbb{Z}^3} \mathbf{d}_{0,\boldsymbol{\xi}} \Phi_{0,\boldsymbol{\xi}}(\mathbf{x}) + \sum_{s=0}^{S-1} \sum_{i=1}^{7} \sum_{\boldsymbol{\xi} \in \mathbb{Z}^3} \mathbf{e}_{s,\boldsymbol{\xi}}^{i} \Psi_{s,\boldsymbol{\xi}}^{i}(\mathbf{x}), \tag{3.8}$$

Table 3.1. Description of DIR-Lab lung scans.

Subject No.	Voxelsize	Dimensions (mm)	Initial mTRE(mm)
1	$0.97 \times 0.97 \times 2.5$	$256 \times 256 \times 94$	3.89
2	$1.16 \times 1.16 \times 2.5$	$256 \times 256 \times 112$	4.34
3	$1.15 \times 1.15 \times 2.5$	$256 \times 256 \times 104$	6.94
4	$1.13 \times 1.13 \times 2.5$	$256 \times 256 \times 99$	9.83
5	$1.10 \times 1.10 \times 2.5$	$256 \times 256 \times 106$	7.48
6	$0.97 \times 0.97 \times 2.5$	$512 \times 512 \times 128$	10.89
7	$0.97 \times 0.97 \times 2.5$	$512 \times 512 \times 136$	11.03
8	$0.97 \times 0.97 \times 2.5$	$512 \times 512 \times 128$	14.99
9	$0.97 \times 0.97 \times 2.5$	$512 \times 512 \times 128$	7.92
10	$0.97 \times 0.97 \times 2.5$	$512 \times 512 \times 120$	7.30

where $\boldsymbol{\xi}$ again represent control points of the FFD grid, i is the index of vector $\boldsymbol{\Psi}(\mathbf{x})$, $\mathbf{d}$ and $\mathbf{e}$ are the coefficient vectors of the scale ($\Phi_{0,\boldsymbol{\xi}}$) and wavelet ($\Psi^i_{s,\boldsymbol{\xi}}$) basis functions, and the parameter vector $\boldsymbol{\nu}$ is formed as $\boldsymbol{\nu} = \{\mathbf{d}_{0,\boldsymbol{\xi}}, \mathbf{e}^i_{0,\boldsymbol{\xi}}, \ldots, \mathbf{e}^i_{S-1,\boldsymbol{\xi}} \mid \boldsymbol{\xi} \in \mathbb{Z}^3, 0 \leq s \leq S-1, i = 1 \ldots 7\}$.

Since the considered Cai-Wang wavelet is expressed in terms of the original B-spline basis function, it follows by substitution of Eq. (3.5) in Eq. (3.8) that the FFD models from Eq. (4.6) and Eq. (3.8) span the same space of deformations. This is also expressed by the equality $V_S = V_0 \oplus W_0 \oplus W_1 \oplus \cdots \oplus W_{S-1}$. This means $\boldsymbol{\nu}$ can be written as a linear transformation of $\boldsymbol{\mu}$

$$\boldsymbol{\nu} = \boldsymbol{P}\boldsymbol{\mu}, \tag{3.9}$$

where the matrix $\boldsymbol{P}$ follows from the substitution. Therefore, the wavelet FFD model is essentially a (linear) reparameterization of the original B-spline FFD model, which has a preconditioning effect on the optimization procedure. An interesting property is also that with the proposed wavelet model, solutions of large norm $\|\boldsymbol{\nu}\|$ will tend to be less smooth than solutions with small norm. For a conventional B-spline FFD model, this does not always hold. For example, $\|\boldsymbol{\mu}\|$ will be large for a global translation of the image.

3.3 Experiments

3.3.1 Image data

Ten 3D chest CT scans of DIR-Lab [15] with 300 manually annotated landmarks in the lung structure were utilized to evaluate the B-spline and wavelet FFD registrations. For the lung data, the exhale phase was registered to the inhale phase. Table 3.1 provides an overview of these scans. To limit the registration to the lung region, lung masks were created by thesholding, 3D-6-neighborhood connected component analysis, and morphological closing operation using a spherical kernel with a diameter of nine voxels.

Besides the lung data, 18 T1-weighted MRI 3D brain scans of Internet Brain Segmentation Repository (IBSR v2.0) [103] were used to evaluate the B-spline and wavelet FFD registrations. These brain scans have been positionally transformed into Talairach space [102] and have been processed by the CMA (Center for Morphometric Analysis) bias field correction routines [16]. The voxel sizes are divided into three groups (8: $0.94 \times 0.94 \times 1.5$, 6: $0.84 \times 0.84 \times 1.5$, 4: $1 \times 1 \times 1.5$). The volumes of these images are $256 \times 256 \times 128$mm. For the brain data, 18×17 inter-subject registrations were tested.

3.3.2   Registration settings

The open source image registration package `elastix` [47] was used to implement this work. The sum of squared intensity differences (SSD) and the normalized correlation coefficient (NCC) were used as the (dis)similarity metrics on lung and brain data, respectively. We used a nonlinear conjugate gradient optimizer (NCG) [22, 48] as the optimization method. The number of iterations was limited to 100 per registration phase. A common hierarchical multiresolution strategy was employed, increasing S in each registration phase, and thereby the degrees of freedom of the FFD models $\mathbf{T}_{\boldsymbol{\mu}}^{S}(\mathbf{x})$ and $\mathbf{T}_{\boldsymbol{\nu}}^{S}(\mathbf{x})$. Note that in the wavelet model, the transformation levels $0 \le s \le S-1$ are optimized simultaneously. In all experiments, resolution levels $s = [0, 3]$ were used. The image scale stacks were generated using $\{\sigma_0, \ldots, \sigma_S\} = \{4, 2, 1, 0.5\}$ voxels. In the CT lung experiments, the finest grid spacing g_S was set to 8mm, 10mm, 13mm, or 16mm, isotropically. In the MRI brain experiments, g_S was set to 3mm, isotropically.

3.3.3   Evaluation measures

The mean target registration error (mTRE) was used to evaluate the registration accuracy on lung data, which calculates the mean distance between the ground truth and registered landmarks. The mTRE can be calculated as

$$\text{mTRE} = \frac{1}{n} \sum_{i=1}^{n} \| \mathbf{T}(\mathbf{p}_i^F) - \mathbf{p}_i^M \|, \tag{3.10}$$

where $\mathbf{p}_i^F$ and $\mathbf{p}_i^M$ represent the corresponding ground truth landmarks in fixed and moving images, respectively. $n = 300$ is the number of landmarks in all test cases.

In the brain data, 84 manually labeled regions are available. With these labels we can use mean overlap (MO) to measure the registration accuracy

$$\text{Mean Overlap} = 2 \frac{\sum_r | M_r \bigcap F_r |}{\sum_r (| M_r | + | F_r |)}, \tag{3.11}$$

where r represents a certain label, and the MO is calculated over all labels.

Besides the accuracy, the smoothness of transformation is an important measure to evaluate the performance of a registration method. In this work, the determinant of spatial Jacobian D_{SJ} was used to measure the smoothness of the transformation

$$D_{SJ} = \left| \frac{\partial \mathbf{T}}{\partial \boldsymbol{x}}(\tilde{\boldsymbol{x}}) \right|. \tag{3.12}$$

For a given spatial location $\tilde{x}$, D_{SJ} calculates the degree of local deformation around it. In a smooth transformation field, the fluctuation of D_{SJ} will be relatively small. Therefore, we utilized the standard deviation of D_{SJ} over the whole 3D image to represent the smoothness of the deformation field.

3.4   Results

Figure 3.3 (a) shows the registration accuracy by B-splines and wavelet based FFD registrations on CT lung data. Wavelet FFD registration produced lower mTRE than B-spline FFD registration for all control point spacings g_S. From Figure 3.3 (a) the mTRE for both B-spline and wavelet models increased with decreasing g_S. In the absence of any additional regularization terms, the decreasing g_S causes an unregularized deformation field. This is the reason why the registration accuracy is decreased with smaller finest grid spacing. However, the accuracy of wavelet is consistently better than B-splines with different finest grid spacings. Besides the comparison of accuracy, Figure 3.3 (b) shows the results of transformation smoothness. Here we see that B-spline FFD registration with all different control point spacing g_S yielded less smooth deformations than the wavelet based FFD registration.
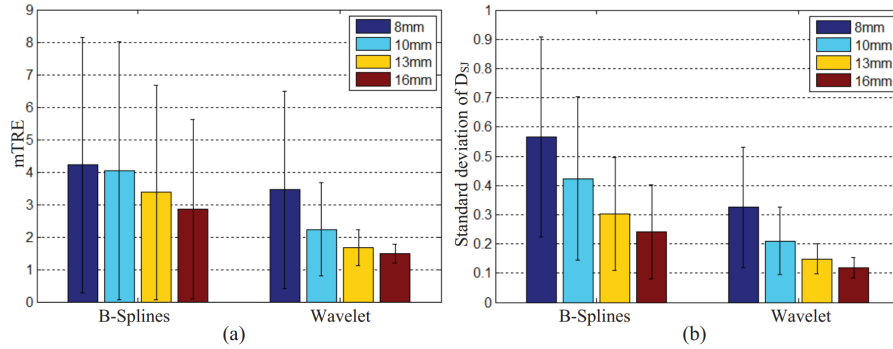
Figure 3.3. Lung data: (a) mean and standard deviation of mTRE on 10 datasets using four different g_S; (b) mean and standard deviation of the determinant of D_{SJ} on 10 datasets using four different g_S.

Figure 3.4 provides the registration accuracy and smoothness on brain data. Here, we only evaluated the performances of B-splines and wavelet using the finest grid spacing 3mm because the intersubject registration has a large number (306) of test cases. From Figure 3.4 (a), wavelet produced better registration accuracy than B-splines. For the smoothness of transformation, Figure 3.4 (b) shows that B-splines generated worse smoothness than the smoothness by wavelet. Therefore, the results on brain data further confirm the results on lung data.
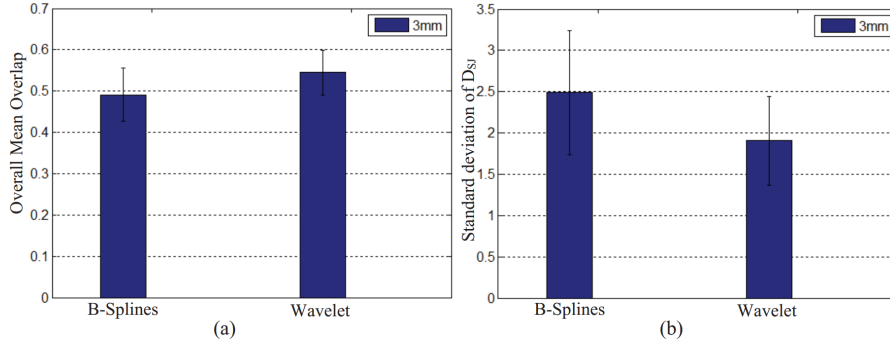
Figure 3.4. Brain data: (a) mean and standard deviation of MO on 306 test cases using $g_S = 3mm$; (b) mean and standard deviation of the determinant of D_{SJ} on 306 test cases using $g_S = 3mm$.

3.5 Conclusion

In this work, we investigate whether a wavelet-based FFD model has advantages for nonrigid image registration. From the results on 10 CT lung and 18 T1-weighted MRI brain datasets, wavelet model produced better accuracy than B-spline model using all different finest grid spacings g_S. For registration smoothness, wavelet model also generated smoother transformation field than B-spline with different g_S.

Theoretically, the B-spline and the wavelet models span the same space of deformations. Yet, the experimental results are different. A potential explanation of this lies in the preconditioning effect of the wavelet parameterization, which may yield an implicit regularization. In the absence of any additional regularization terms, the original B-spline FFD registration may produce worse results with decreasing grid spacing. The wavelet based FFD registration appears more robust in this case.

In future work, the performance of wavelet based FFD registration in combination with different multiresolution strategies for registration [?, 98] will be investigated.

Discussion and conclusion

To make optimal use of medical imaging data, advanced medical image processing and analysis tools are needed, e.g., for the computation of quantitative imaging biomarkers, creation of anatomical and functional models, combination of multimodal images, and comparison of baseline and follow-up images. Image registration is one of the essential techniques in medical image processing, and is widely applied both in supporting biomedical research and clinical practice. In this thesis, we address different components of a registration framework, to improve registration robustness, accuracy and speed. Specifically, our contributions cover different multiresolution strategies, transformation models and optimization algorithms used in image registration. The above components directly influence the performance of a registration approach.

In Chapter 2 we focused on various multiresolution strategies in image registration. In comparison to a conventional step-by-step hierarchical strategy, several novel simultaneous multiresolution strategies were presented. If the low and high resolution levels of data are combined to guide the optimization, large-scale and small-scale image information can be considered simultaneously. Similarly, a simultaneous multiresolution strategy for the transformation model can be employed to distribute the whole deformation over different resolution levels of the transformation model. Ideally, large deformations should be represented by a coarser transformation level, and remaining smaller deformations should be captured by the finer transformation levels. We implemented all methods using free-form deformations (FFD) with B-spline registration [85]. In our evaluation experiments, we used publicly available computed tomography (CT) lung and T1-weighted magnetic resonance imaging (MRI) brain data. The performance of the different multiresolution strategies was evaluated in terms of both registration accuracy and transformation smoothness. It was found that a simultaneous multiresolution strategy of data can enhance registration accuracy, and a hierarchically simultaneous transformation strategy leads to smoother transformations. In different applications, registration accuracy and smoothness may have different importance and therefore we cannot conclude which combination is to be preferred in general. Nevertheless, for both registration accuracy and transformation smoothness, the method with hierarchically simultaneous transformation and simultaneous data strategies is a better choice than the traditionally hierarchical registration strategy.

In Chapter 3 we investigated whether a wavelet-based FFD model has advantages for nonrigid image registration. Using wavelets, we can decompose signal into different scales in a unique manner. To be used in the setting of a nonrigid transformation model, the wavelet should be differentiable, compactly supported and orthogonal

between different scales. Cai and Wang [13] proposed a B-splines based wavelet model which fulfills our requirements in Sobolev space. We used a nonlinear conjugate gradient (NCG) optimizer [22, 48] as the optimization method. In experiments on 10 CT lung and 18 T1-weighted MRI brain datasets, the results obtained with the wavelet model were more accurate than with the B-spline model. With respect to smoothness of the resulting deformation, the wavelet model also generated smoother transformation field than B-spline model. Theoretically, the B-spline and the wavelet models span the same space of deformations. However, the experimental results were different. A potential explanation of this lies in the preconditioning effect of the wavelet parameterization, which may yield an implicit regularization. In the absence of any additional regularization terms, the original B-spline FFD registration may produce worse results with decreasing grid spacing. The wavelet based FFD registration appears more robust in this case. It would be interesting in future work to evaluate the wavelet transformation also in combination with SGD methods. A challenge here is that the current implementation of the initial step size estimation in adaptive stochastic gradient descent (ASGD) is not optimal for use in combination with the wavelet transformation model, leading to high computational cost. A possible solution for this would be to use the fast ASGD optimizer proposed in [80].

Chapter 4 explored the use of lower-order B-splines. Inspired by the convolutional definition of B-splines, we proposed to apply a random perturbation process to an mth-order B-spline to approximate the original nth-order B-spline transformation with $m \leq n$. The new randomly perturbed FFD (RPFFD) registration method is embedded in an SGD-based registration framework [48]. By using the mth-order B-spline rather than the original nth-order B-spline, the computational cost is inherently reduced by a factor $\left(\frac{m+1}{n+1}\right)^D$ thanks to the smaller support region and hence less control points are involved in the computation. We evaluated the proposed method for a range of B-spline of orders m and n. Experiments on simulated 2D brain data with artificial deformations were performed to validate the registration accuracy in a setting with known ground truth. Publicly available 3D lung CT and brain MRI scans were used to verify the registration performance on real data. Methods were compared in terms of registration accuracy, transformation smoothness, and computational efficiency. Experimental results indicated that the proposed RPFFD method outperforms the standard third-order FFD method in terms of the registration accuracy and transformation smoothness. Besides the expected lower computational cost of lower-order B-splines, it is interesting to observe that the first- and second-order B-splines equipped with the random perturbation technique can achieve competitive or even better registration accuracy and transformation smoothness than the third-order B-spline. Possible explanations for this result were provided in the discussion of Chapter 4.

Chapter 5 tackled the problem of getting stuck in local minima during the optimization procedure of image registration. Local minima in the optimization landscape can potentially be eliminated by smoothing the cost function. Multiresolution strategies indirectly achieve some sort of cost function smoothing by blurring the images, but in our approach we investigated the effect of directly smoothing the cost function. Conceptually, a straightforward way to smooth the cost function would be by convolving with a smoothing kernel in the transformation parameter space. However,

a major challenge here is the high dimensionality of the parameter space. Inspired by [26], we proposed to inject Gaussian random noise into the transformation parameters during the optimization process of image registration. In contrast to the costly multi-start algorithm by [39], which applies multiple perturbations to the initial transformation parameters, one (or just a few) random perturbation(s) is applied to the transformation parameters in each iteration. This randomized smoothing (RS) technique is combined with a SGD optimizer [45], which can naturally deal with the random perturbations. The RS method could be seen as a computationally efficient way that implicitly smooths the cost function, thus eliminating local minima in the optimization landscape. In Chapter 5, translation, rigid, affine and nonrigid B-spline transformation models were used in the validation. Experiments on two-dimensional artificial images, two-dimensional cell images, three-dimensional lung CT, and brain MRI scans were carried out to evaluate the effectiveness of the RS registration approach. The improvement in registration results proves the effectiveness of the RS technique.

In Chapter 6, we proposed to use a constant optimization step size (instead of a gradually decreasing step size), in combination with an iterative averaging technique, to improve the overall convergence speed. In SGD optimization, stochastic approximations of the cost function derivative are used in each iteration to update the transformation parameters. The stochastic approximation error leads to randomness in the parameters. Therefore, convergence has to be enforced by gradually decreasing the update step size. Polyak and Juditsky [79] proved that by simply averaging of the parameters obtained by the SGD optimizer over several iterations, the highest possible rate of convergence can be achieved. Therefore, we proposed an averaged SGD (Avg-SGD) method for efficient image registration. For the Avg-SGD approach, a constant step sequence of optimization could be used without sacrificing the registration precision. We provided two definitions of the Avg-SGD method: postponed and exponential. For the postponed definition the first k_0 iterates are skipped in computing the averaged $\boldsymbol{\mu}$. In the exponential definition, the effects of the early iterations are exponentially decreased, avoiding the need to set a hard threshold k_0. The Avg-SGD method is suitable for both rigid and nonrigid registration problems. Experiments on simulated 2D brain MRI data and real 3D lung CT scans demonstrate the effectiveness of the Avg-SGD method in terms of convergence rate and registration precision.

In summary this thesis introduced a number of improvements to different components of the registration methodology. All proposed new approaches were evaluated in extensive experiments, including both synthetic and public real biomedical data, and comparisons with state-of-the-art conventional methods were made.

The methodological contributions are in principle independent of each other, so they could be combined if desired in particular applications. For example, Chapter 5 introduced the RS technique for suppressing local minima of the cost function. The RS technique involves the injection of random Gaussian noise into the transformation parameters at each iteration. This added noise may enlarge the randomness of the SGD optimization, leading to reduced precision. By averaging the iterates of optimization, i.e., using the Avg-SGD method as proposed in Chapter 6, we could compensate for the amplified noise, while maintaining or even accelerating conver-

gence rate. In Chapter 5, it was found that in some applications we need to average multiple sets of perturbations in each iteration to alleviate the effect of large Gaussian noise. However, the computation time of registration scales directly with the number of averages. In contrast, the Avg-SGD requires almost no additional computation time. No additional cost function gradient evaluations are needed. The averaging over iterates is implemented in an efficient recursive way, which requires only one additional vector of transformation parameters to be stored during optimization. Thus, the computational cost could be reduced substantially by applying the Avg-SGD approach to the RS technique.

As another example, multi-level B-spline FFD is utilized in Chapter 2 to model simultaneous multiresolution strategies. The computational cost is increased in the hierarchically simultaneous transformation. To avoid this disadvantage, Chapter 4 proposes to use more efficient lower-order B-splines to approximate higher-order B-splines by using the novel random perturbation technique. Therefore, one solution could be that we adopt the randomly perturbed first-order B-spline to model the multi-level B-spline FFD for the hierarchically simultaneous transformation. In this way, we may create a new registration approach which balances registration accuracy and computational efficiency.

The methods proposed in this thesis do not make use of domain-specific knowledge, and can thus be used in a wide variety of applications. In this thesis, we evaluated the performances of the proposed registration methods mostly based on public CT and MRI data. It could be interesting to validate the new techniques also on other types of medical imaging data, such as ultrasound and positron emission tomography (PET). Meanwhile, the new methods can be applied to more anatomical structures, e.g., liver, prostate, etc.

In this thesis we focus on the methodological parts of the medical image registration. In-depth clinical evaluations and use of the proposed registration methods is an important future direction of research. This is facilitated, as all of the new techniques will be publicly available as part of the open source registration package `elastix`.

Bibliography

[1] Jacob Abernethy, Chansoo Lee, Abhinav Sinha, Ambuj Tewari, "Online Linear Optimization via Smoothing", in *The 27th Conference on Learning Theory*, pp. 807–823, 2014.

[2] Iman Aganj, BT Thomas Yeo, Mert R Sabuncu, Bradley Fischl, "On removing interpolation and resampling artifacts in rigid image registration", *IEEE Transactions on Image Processing*, vol. 22, no. 2, pp. 816–827, 2013.

[3] Shun-Ichi Amari, Hyeyoung Park, Kenji Fukumizu, "Adaptive method of realizing natural gradient learning for multilayer perceptrons", *Neural Computation*, vol. 12, no. 6, pp. 1399–1409, 2000.

[4] Amir Beck & Marc Teboulle, "Smoothing and first order methods: A unified framework", *SIAM Journal on Optimization*, vol. 22, no. 2, pp. 557–580, 2012.

[5] D. P. Bertsekas, *Nonlinear programming*, Athena Scientific, 1999.

[6] P.J. Besl & Neil D. McKay, "A method for registration of 3-D shapes", *IEEE Transactions on Pattern Analysis and Machine Intelligence*, vol. 14, no. 2, pp. 239–256, Feb 1992.

[7] Roshni Bhagalia, Jeffrey Fessler, Boklye Kim, others, "Accelerated nonrigid intensity-based image registration using importance sampling", *IEEE Transactions on Medical Imaging*, vol. 28, no. 8, pp. 1208–1216, 2009.

[8] Antoine Bordes, Léon Bottou, Patrick Gallinari, "SGD-QN: Careful quasi-Newton stochastic gradient descent", *The Journal of Machine Learning Research*, vol. 10, pp. 1737–1754, 2009.

[9] Léon Bottou, "Large-scale machine learning with stochastic gradient descent", in *Proceedings of COMPSTAT'2010*, Springer, pp. 177–186, 2010.

[10] Léon Bottou & Yann Le Cun, "On-line learning for very large data sets", *Applied Stochastic Models in Business and Industry*, vol. 21, no. 2, pp. 137–151, 2005.

[11] Olivier Bousquet & Léon Bottou, "The tradeoffs of large scale learning", in *Advances in Neural Information Processing Systems*, pp. 161–168, 2008.

[12] Richard H Byrd, SL Hansen, Jorge Nocedal, Yoram Singer, "A stochastic quasi-Newton method for large-scale optimization", *arXiv preprint arXiv:1401.7020*, 2014.

[13] Wei Cai & Jianzhong Wang, "Adaptive multiresolution collocation methods for initial-boundary value problems of nonlinear PDEs", *SIAM Journal on Numerical Analysis*, vol. 33, no. 3, pp. 937–970, 1996.

[14] Noemí Carranza-Herrezuelo, A Bajo, Filip Sroubek, C Santamarta, Gabriel Cristóbal, Andrés Santos, María J Ledesma-Carbayo, "Motion estimation of tagged cardiac magnetic resonance images using variational techniques", *Computerized Medical Imaging and Graphics*, vol. 34, no. 6, pp. 514–522, 2010.

[15] R. Castillo, E. Castillo, R. Guerra, V. E. Johnson, T. McPhail, A. K. Garg, T. Guerrero, "A framework for evaluation of deformable image registration spatial accuracy using large landmark point sets", *Physics in Medicine and Biology*, vol. 54, no. 7, pp. 1849–1870, 2009.

[16] Verne S Caviness, Joachim Meyer, Nikos Makris, David N Kennedy, "MRI-based topographic parcellation of human neocortex: an anatomically specified method with estimate of reliability", *Cognitive Neuroscience, Journal of*, vol. 8, no. 6, pp. 566–587, 1996.

[17] Haili Chui & Anand Rangarajan, "A new point matching algorithm for non-rigid registration", *Computer Vision and Image Understanding*, vol. 89, no. 2, pp. 114–141, 2003.

[18] Se Young Chun & Jeffrey A Fessler, "A simple regularizer for B-spline nonrigid image registration that encourages local invertibility", *IEEE Journal of Selected Topics in Signal Processing*, vol. 3, no. 1, pp. 159–169, 2009.

[19] Chris A. Cocosco, Vasken Kollokian, Remi K.-S. Kwan, G. Bruce Pike, Alan C. Evans, "BrainWeb: Online Interface to a 3D MRI Simulated Brain Database", *NeuroImage*, vol. 5, p. 425, 1997.

[20] W. R. Crum, T. Hartkens, D. L. G. Hill, "Non-rigid image registration: theory and practice", *British Journal of Radiology*, vol. 77, no. suppl 2, pp. S140–S153, 2004.

[21] W R Crum, T Hartkens, D L G Hill, "Non-rigid image registration: theory and practice", *The British Journal of Radiology*, vol. 77, no. suppl_2, pp. S140–S153, 2004.

[22] Yu-Hong Dai, "A family of hybrid conjugate gradient methods for unconstrained optimization", *Mathematics of Computation*, vol. 72, no. 243, pp. 1317–1328, 2003.

[23] Carl De Boor, *A practical guide to splines*, vol. 27, Springer-Verlag New York, 1978.

[24] Marius de Groot, Meike W Vernooij, Stefan Klein, M Arfan Ikram, Frans M Vos, Stephen M Smith, Wiro J Niessen, Jesper LR Andersson, "Improving alignment in tract-based spatial statistics: evaluation and optimization of image registration", *NeuroImage*, vol. 76, pp. 400–411, 2013.

[25] JrJohn E Dennis & Jorge J Moré, "Quasi-Newton methods, motivation and theory", *SIAM review*, vol. 19, no. 1, pp. 46–89, 1977.

[26] John C Duchi, Peter L Bartlett, Martin J Wainwright, "Randomized smoothing for stochastic optimization", *SIAM Journal on Optimization*, vol. 22, no. 2, pp. 674–701, 2012.

[27] B. Fischer & J. Modersitzki, "Ill-posed medicine–an introduction to image registration", *Inverse Problems*, vol. 24, no. 3, p. 034008, 2008.

[28] Valerio Fortunati, René F Verhaart, Fedde van der Lijn, Wiro J Niessen, Jifke F Veenland, Margarethus M Paulides, Theo van Walsum, "Tissue segmentation of head and neck CT images for treatment planning: a multiatlas approach combined with intensity modeling", *Medical Physics*, vol. 40, no. 7, p. 071905, 2013.

[29] Peisheng Gao & Thomas W Sederberg, "A work minimization approach to image morphing", *The Visual Computer*, vol. 14, no. 8, pp. 390–400, 1998.

[30] Saul B Gelfand & Sanjoy K Mitter, "Recursive stochastic algorithms for global optimization in R^d", *SIAM Journal on Control and Optimization*, vol. 29, no. 5, pp. 999–1018, 1991.

[31] Rajarshi P Ghosh, Rachel A Horowitz-Scherer, Tatiana Nikitina, Luda S Shlyakhtenko, Christopher L Woodcock, "MeCP2 binds cooperatively to its substrate and competes with histone H1 for chromatin binding sites", *Molecular and cellular biology*, vol. 30, no. 19, pp. 4656–4670, 2010.

[32] Nikolaus Hansen & Andreas Ostermeier, "Completely derandomized self-adaptation in evolution strategies", *Evolutionary Computation*, vol. 9, no. 2, pp. 159–195, 2001.

[33] Rolf A Heckemann, Joseph V Hajnal, Paul Aljabar, Daniel Rueckert, Alexander Hammers, "Automatic anatomical brain MRI segmentation combining label propagation and decision fusion", *NeuroImage*, vol. 33, no. 1, pp. 115–126, 2006.

[34] Mattias P Heinrich, Mark Jenkinson, Michael Brady, Julia A Schnabel, "Globally Optimal Deformable Registration on a Minimum Spanning Tree Using Dense Displacement Sampling", *Medical Image Computing and Computer-Assisted Intervention–MICCAI 2012*, pp. 115–122, 2012.

[35] D. L. G. Hill, P. G. Batchelor, M. Holden, D. J. Hawkes, "Medical image registration", *Physics in Medicine and Biology*, vol. 46, no. 3, pp. R1–R45, 2001.

[36] M. Holden, "A review of geometric transformations for nonrigid body registration", *IEEE Transactions on Medical Imaging*, vol. 27, no. 1, pp. 111–128, 2008.

[37] M. Hollander & D. A. Wolfe, "Nonparametric statistical methods", 1999.

[38] Mark Jenkinson, Peter Bannister, Michael Brady, Stephen Smith, "Improved optimization for the robust and accurate linear registration and motion correction of brain images", *NeuroImage*, vol. 17, no. 2, pp. 825–841, 2002.

[39] Mark Jenkinson & Stephen Smith, "A global optimisation method for robust affine registration of brain images", *Medical Image Analysis*, vol. 5, no. 2, pp. 143–156, 2001.

[40] Bing Jian & Baba C Vemuri, "Robust point set registration using gaussian mixture models", *IEEE Transactions on Pattern Analysis and Machine Intelligence*, vol. 33, no. 8, pp. 1633–1645, 2011.

[41] Jack Kiefer & Jacob Wolfowitz, "Stochastic estimation of the maximum of a regression function", *The Annals of Mathematical Statistics*, vol. 23, no. 3, pp. 462–466, 1952.

[42] Hortense A Kirisli, Michiel Schaap, Stefan Klein, Lisan A Neefjes, Annick C Weustink, Theo Van Walsum, Wiro J Niessen, "Fully automatic cardiac segmentation from 3D CTA data: a multi-atlas based approach", in *SPIE Medical Imaging*, International Society for Optics and Photonics, pp. 762305–762305, 2010.

[43] Arno Klein, Jesper Andersson, Babak A Ardekani, John Ashburner, Brian Avants, Ming-Chang Chiang, Gary E Christensen, D Louis Collins, James Gee, Pierre Hellier, others, "Evaluation of 14 nonlinear deformation algorithms applied to human brain MRI registration", *NeuroImage*, vol. 46, no. 3, pp. 786–802, 2009.

[44] A. Klein, J. Andersson, B. A. Ardekani *et al.*, "Evaluation of 14 nonlinear deformation algorithms applied to human brain MRI registration", *NeuroImage*, vol. 46, pp. 786–802, 2009.

[45] S. Klein, J. P. W. Pluim, M. Staring, M. A. Viergever, "Adaptive stochastic gradient descent optimisation for image registration", *International Journal of Computer Vision*, vol. 81, no. 3, pp. 227–239, 2009.

[46] Stefan Klein, Marius Staring, Patrik Andersson, Josien PW Pluim, "Preconditioned stochastic gradient descent optimisation for monomodal image registration", in *Medical Image Computing and Computer-Assisted Intervention–MICCAI 2011*, Springer, pp. 549–556, 2011.

[47] S. Klein, M. Staring, K. Murphy, M. A. Viergever, J. P. W. Pluim, "Elastix: a toolbox for intensity-based medical image registration", *IEEE Transactions on Medical Imaging*, vol. 29, no. 1, pp. 196–205, 2010.

[48] S. Klein, M. Staring, J. P. W. Pluim, "Evaluation of optimization methods for nonrigid medical image registration using mutual information and B-splines", *IEEE Transactions on Image Processing*, vol. 16, no. 12, pp. 2879–2890, 2007.

[49] Stefan Klein, Uulke A van der Heide, Irene M Lips, Marco van Vulpen, Marius Staring, Josien PW Pluim, "Automatic segmentation of the prostate in 3D MR images by atlas matching using localized mutual information", *Medical Physics*, vol. 35, no. 4, pp. 1407–1417, 2008.

[50] Vikram Krishnamurthy, "Averaged stochastic gradient algorithms for adaptive blind multiuser detection in DS/CDMA systems", *IEEE Transactions on Communications*, vol. 48, no. 1, pp. 125–134, 2000.

[51] HJ Kushner, "Asymptotic global behavior for stochastic approximation and diffusions with slowly decreasing noise effects: global minimization via Monte Carlo", *SIAM Journal on Applied Mathematics*, vol. 47, no. 1, pp. 169–185, 1987.

[52] Harold J Kushner & George Yin, *Stochastic approximation and recursive algorithms and applications*, vol. 35, Springer Science & Business Media, 2003.

[53] Jan Kybic & Michael Unser, "Fast parametric elastic image registration", *IEEE Transactions on Image Processing*, vol. 12, no. 11, pp. 1427–1442, 2003.

[54] Thomas M Lehmann, Claudia Gönner, Klaus Spitzer, "Survey: Interpolation methods in medical image processing", *IEEE Transactions on Medical Imaging*, vol. 18, no. 11, pp. 1049–1075, 1999.

[55] H. Lester & S. R. Arridge, "A survey of hierarchical non-linear medical image registration", *Pattern Recognition*, vol. 32, no. 1, pp. 129 – 149, 1999.

[56] Hava Lester & Simon R Arridge, "A survey of hierarchical non-linear medical image registration", *Pattern Recognition*, vol. 32, no. 1, pp. 129–149, 1999.

[57] Bostjan Likar & Franjo Pernuš, "A hierarchical approach to elastic registration based on mutual information", *Image and Vision Computing*, vol. 19, no. 1, pp. 33–44, 2001.

[58] S. Lu, S. V. Pereverzev, R. Ramlau, "An analysis of Tikhonov regularization for nonlinear ill-posed problems under a general smoothness assumption", *Inverse Problems*, vol. 23, no. 1, p. 217, 2006.

[59] Frederik Maes, Andre Collignon, Dirk Vandermeulen, Guy Marchal, Paul Suetens, "Multimodality image registration by maximization of mutual information", *IEEE Transactions on Medical Imaging*, vol. 16, no. 2, pp. 187–198, 1997.

[60] Frederik Maes, Dirk Vandermeulen, Paul Suetens, "Comparative evaluation of multiresolution optimization strategies for multimodality image registration by maximization of mutual information", *Medical Image Analysis*, vol. 3, no. 4, pp. 373–386, 1999.

[61] J.B.Antoine Maintz & Max A. Viergever, "A survey of medical image registration", *Medical Image Analysis*, vol. 2, no. 1, pp. 1 – 36, 1998.

[62] Pravat K Mandal, Rashima Mahajan, Ivo D Dinov, "Structural brain atlases: design, rationale, and applications in normal and pathological cohorts", *Journal of Alzheimer's Disease*, vol. 31, no. 0 3, pp. 169–188, 2012.

[63] John L Maryak & Daniel C Chin, "Global random optimization by simultaneous perturbation stochastic approximation", in *Proceedings of the American Control Conference*, vol. 2, IEEE, pp. 756–762, 2001.

[64] David Mattes, David R Haynor, Hubert Vesselle, Thomas K Lewellen, William Eubank, "PET-CT image registration in the chest using free-form deformations", *IEEE Transactions on Medical Imaging*, vol. 22, no. 1, pp. 120–128, 2003.

[65] Erik Meijering, "A chronology of interpolation: from ancient astronomy to modern signal and image processing", *Proceedings of the IEEE*, vol. 90, no. 3, pp. 319–342, 2002.

[66] C. T. Metz, S. Klein, M. Schaap, T. Van Walsum, W. J. Niessen, "Nonrigid registration of dynamic medical imaging data using nD+t B-splines and a groupwise optimization approach", *Medical Image Analysis*, vol. 15, no. 2, pp. 238–249, 2011.

[67] Marc Modat, Gerard R Ridgway, Zeike A Taylor, Manja Lehmann, Josephine Barnes, David J Hawkes, Nick C Fox, Sébastien Ourselin, "Fast free-form deformation using graphics processing units", *Computer Methods and Programs in Biomedicine*, vol. 98, no. 3, pp. 278–284, 2010.

[68] K. Murphy & *et al.*, "Evaluation of registration methods on thoracic CT: the EMPIRE10 challenge", *IEEE Transactions on Medical Imaging*, vol. 30, no. 11, pp. 1901–1920, Nov 2011.

[69] K. Murphy, B. Van Ginneken, J. M. Reinhardt, S. Kabus, K. Ding, X. Deng, K. Cao, K. Du, G. E. Christensen, V. Garcia, others, "Evaluation of registration methods on thoracic CT: The EMPIRE10 challenge", *IEEE Transactions on Medical Imaging*, vol. 30, no. 11, pp. 1901–1920, 2011.

[70] Arkadiĭ Semenovich Nemirovsky & David Borisovich Yudin, *Problem complexity and method efficiency in optimization*, Wiley, 1983.

[71] Yu Nesterov, "Smooth minimization of non-smooth functions", *Mathematical Programming*, vol. 103, no. 1, pp. 127–152, 2005.

[72] Vincent Noblet, Christian Heinrich, Fabrice Heitz, J P Armspach, "3-D deformable image registration: a topology preservation scheme based on hierarchical deformation models and interval analysis optimization", *IEEE Transactions on Image Processing*, vol. 14, no. 5, pp. 553–566, 2005.

[73] Jorge Nocedal & Stephen J Wright, *Numerical optimization*, New York: Springer-Verlag, 1999.

[74] Bartłomiej W Papież, Mattias P Heinrich, Jérome Fehrenbach, Laurent Risser, Julia A Schnabel, "An implicit sliding-motion preserving regularisation via bilateral filtering for deformable image registration", *Medical Image Analysis*, vol. 18, no. 8, pp. 1299 – 1311, 2014.

[75] Bartłomiej W Papież, Mattias P Heinrich, Jérome Fehrenbach, Laurent Risser, Julia A Schnabel, "An implicit sliding-motion preserving regularisation via bilateral filtering for deformable image registration", *Medical Image Analysis*, vol. 18, no. 8, pp. 1299–1311, 2014.

[76] S. Pereverzev & E. Schock, "On the adaptive selection of the parameter in regularization of ill-posed problems", *SIAM Journal on Numerical Analysis*, vol. 43, no. 5, pp. 2060–2076, 2005.

[77] Josien PW Pluim, JB Antoine Maintz, Max A Viergever, "Interpolation artefacts in mutual information-based image registration", *Computer Vision and Image Understanding*, vol. 77, no. 2, pp. 211–232, 2000.

[78] Josien PW Pluim, JB Antoine Maintz, Max A Viergever, "Mutual-information-based registration of medical images: a survey", *IEEE Transactions on Medical Imaging*, vol. 22, no. 8, pp. 986–1004, 2003.

[79] Boris T Polyak & Anatoli B Juditsky, "Acceleration of stochastic approximation by averaging", *SIAM Journal on Control and Optimization*, vol. 30, no. 4, pp. 838–855, 1992.

[80] Y Qiao, BPF Lelieveldt, M Staring, "Fast automatic estimation of the optimization step size for nonrigid image registration", in *SPIE Medical Imaging*, International Society for Optics and Photonics, pp. 90341A–90341A, 2014.

[81] S. Ramani, Z. Liu, J. Rosen, J. Nielsen, J. A. Fessler, "Regularization parameter selection for nonlinear iterative image restoration and MRI reconstruction using GCV and SURE-based methods", *IEEE Transactions on Image Processing*, vol. 21, no. 8, pp. 3659–3672, 2012.

[82] Herbert Robbins & Sutton Monro, "A stochastic approximation method", *The Annals of Mathematical Statistics*, pp. 400–407, 1951.

[83] T. Rohlfing, "Image similarity and tissue overlaps as surrogates for image registration accuracy: widely used but unreliable", *IEEE Transactions on Medical Imaging*, vol. 31, no. 2, pp. 153–163, 2012.

[84] Daniel Rueckert, Paul Aljabar, Rolf A Heckemann, Joseph V Hajnal, Alexander Hammers, "Diffeomorphic registration using B-splines", in *Medical Image Computing and Computer-Assisted Intervention–MICCAI*, Springer, pp. 702–709, 2006.

[85] D. Rueckert, L. I. Sonoda, C. Hayes *et al.*, "Nonrigid Registration Using Free-Form Deformations: Application to Breast MR Images", *IEEE Transactions on Medical Imaging*, vol. 18, no. 8, pp. 712 – 721, 1999.

[86] David Ruppert, "Efficient estimations from a slowly convergent Robbins-Monro process", Tech. Rep., Cornell University Operations Research and Industrial Engineering, 1988.

[87] Nicol N Schraudolph, Jin Yu, Simon Günter, "A stochastic quasi-Newton method for online convex optimization", in *International Conference on Artificial Intelligence and Statistics*, pp. 436–443, 2007.

[88] Denis P Shamonin, Esther E Bron, Boudewijn PF Lelieveldt, Marion Smits, Stefan Klein, Marius Staring *et al.*, "Fast parallel image registration on CPU and GPU for diagnostic classification of Alzheimer's disease", *Frontiers in Neuroinformatics*, vol. 7, 2013.

[89] Wenzhe Shi, Martin Jantsch, Paul Aljabar, Luis Pizarro, Wenjia Bai, Haiyan Wang, Declan ORegan, Xiahai Zhuang, Daniel Rueckert, "Temporal sparse free-form deformations", *Medical Image Analysis*, vol. 17, no. 7, pp. 779–789, 2013.

[90] W. Shi, X. Zhuang, L. Pizarro, W. Bai, H. Wang, K. P. Tung, P. Edwards, D. Rueckert, "Registration Using Sparse Free-Form Deformations", *Medical Image Computing and Computer-Assisted Intervention–MICCAI 2012*, pp. 659–666, 2012.

[91] Ihor Smal, Noemí Carranza-Herrezuelo, Stefan Klein, Piotr Wielopolski, Adriaan Moelker, Tirza Springeling, Monique Bernsen, Wiro Niessen, Erik Meijering, "Reversible jump MCMC methods for fully automatic motion analysis in tagged MRI", *Medical Image Analysis*, vol. 16, no. 1, pp. 301–324, 2012.

[92] S. Somayajula, A. A. Joshi, R. M. Leahy, "Mutual information based non-rigidmouse registration using a scale-space approach", in *5th IEEE International Symposium on Biomedical Imaging: From Nano to Macro, 2008. ISBI 2008.*, IEEE, pp. 1147–1150, 2008.

[93] Carlos OS Sorzano, Philippe Thevenaz, Michael Unser, "Elastic registration of biological images using vector-spline regularization", *IEEE Transactions on Biomedical Engineering*, vol. 52, no. 4, pp. 652–663, 2005.

[94] Aristeidis Sotiras, Christos Davatzikos, Nikos Paragios, "Deformable medical image registration: a survey", *IEEE Transactions on Medical Imaging*, vol. 32, no. 7, pp. 1153–1190, 2013.

[95] A. Sotiras, C. Davatzikos, N. Paragios, "Deformable Medical Image Registration: a Survey", *IEEE Transactions on Medical Imaging*, vol. 32, no. 7, pp. 1153–1190, July 2013.

[96] James C Spall, "Multivariate stochastic approximation using a simultaneous perturbation gradient approximation", *IEEE Transactions on Automatic Control*, vol. 37, no. 3, pp. 332–341, 1992.

[97] Wei Sun, W.J. Niessen, M. van Stralen, S. Klein, "Simultaneous Multiresolution Strategies for Nonrigid Image Registration", *IEEE Transactions on Image Processing*, vol. 22, no. 12, pp. 4905–4917, Dec 2013.

[98] Wei Sun, Wiro J. Niessen, Stefan Klein, "Hierarchical vs. Simultaneous Multiresolution Strategies for Nonrigid Image Registration", *Biomedical Image Registration, Lecture Notes in Computer Science*, vol. 7359, pp. 60–69, 2012.

[99] Wei Sun, Wiro J Niessen, Stefan Klein, "Free-form Deformation Using Lower-order B-spline for Nonrigid Image Registration", in *Medical Image Computing and Computer-Assisted Intervention–MICCAI*, Springer, pp. 194–201, 2014.

[100] Wei Sun, Wiro J Niessen, Stefan Klein, "Free-Form Deformation Using Lower-Order B-spline for Nonrigid Image Registration", in *Medical Image Computing and Computer-Assisted Intervention–MICCAI 2014*, Springer, pp. 194–201, 2014.

[101] Wei Sun, Wiro J Niessen, Stefan Klein, "Randomly Perturbed Free-Form Deformation for Nonrigid Image Registration", in *Biomedical Image Registration*, Springer, pp. 62–71, 2014.

[102] J. Talairach & P. Tournoux, *Co-planar stereotaxic atlas of the human brain*, vol. 147, Thieme New York, 1988.

[103] The Internet Brain Segmentation Repository, http://www.nitrc.org/projects/ibsr, ".

[104] Philippe Thévenaz, Michel Bierlaire, Michael Unser, "Halton Sampling for Image Registration Based on Mutual Information", *Sampling Theory Signal Image Process*, vol. 7, no. 2, pp. 141–171, 2006.

[105] Philippe Thévenaz, Thierry Blu, Michael Unser, "Image interpolation and resampling", *Handbook of Medical Imaging, Processing and Analysis*, pp. 393–420, 2000.

[106] Philippe Thévenaz, Thierry Blu, Michael Unser, "Interpolation revisited", *IEEE Transactions on Medical Imaging*, vol. 19, no. 7, pp. 739–758, 2000.

[107] A. W. Toga & P. M. Thompson, "The role of image registration in brain mapping", *Image and Vision Computing*, vol. 19, no. 1, pp. 3–24, 2001.

[108] Dejan Tomazevic, Bostjan Likar, Tomaz Slivnik, Franjo Pernus, "3-D/2-D registration of CT and MR to X-ray images", *IEEE Transactions on Medical Imaging*, vol. 22, no. 11, pp. 1407–1416, 2003.

[109] Jeffrey Tsao, "Interpolation artifacts in multimodality image registration based on maximization of mutual information", *IEEE Transactions on Medical Imaging*, vol. 22, no. 7, pp. 854–864, 2003.

[110] Nicholas J Tustison, Brian B Avants, James C Gee, "Directly manipulated free-form deformation image registration", *IEEE Transactions on Image Processing*, vol. 18, no. 3, pp. 624–635, 2009.

[111] Michael Unser, "Splines: a perfect fit for signal and image processing", *IEEE Signal Processing Magazine*, vol. 16, no. 6, pp. 22–38, 1999.

[112] Michael Unser, Akram Aldroubi, Murray Eden, "B-spline signal processing. I. Theory", *IEEE Transactions on Signal Processing*, vol. 41, no. 2, pp. 821–833, 1993.

[113] Michael Unser, Akram Aldroubi, Murray Eden, "B-spline signal processing. II. Efficiency design and applications", *IEEE Transactions on Signal Processing*, vol. 41, no. 2, pp. 834–848, 1993.

[114] Yoshitaka Ushiku, Mutsuo Hidaka, Tatsuya Harada, "Three Guidelines of Online Learning for Large-Scale Visual Recognition", in *IEEE Conference on Computer Vision and Pattern Recognition (CVPR)*, IEEE, pp. 3574–3581, 2014.

[115] E. B. van de Kraats, G. P. Penney, D. Tomazevic, T. van Walsum, W. J. Niessen, "Standardized evaluation methodology for 2-D-3-D registration", *IEEE Transactions on Medical Imaging*, vol. 24, no. 9, pp. 1177–1189, 2005.

[116] M. Van Stralen & J. P. W. Pluim, "Optimal discrete multi-resolution deformable image registration", in *IEEE International Symposium on Biomedical Imaging: From Nano to Macro, 2009. ISBI'09.*, IEEE, pp. 947–950, 2009.

[117] Mahesh K Varanasi & Deepak Das, "Fast stochastic power control algorithms for nonlinear multiuser receivers", *IEEE Transactions on Communications*, vol. 50, no. 11, pp. 1817–1827, 2002.

[118] Paul Viola & William M Wells III, "Alignment by maximization of mutual information", *International Journal of Computer Vision*, vol. 24, no. 2, pp. 137–154, 1997.

[119] Yu-Te Wu, Takeo Kanade, Ching-Chung Li, Jeffrey Cohn, "Image registration using wavelet-based motion model", *International Journal of Computer Vision*, vol. 38, no. 2, pp. 129–152, 2000.

[120] Wei Xu, "Towards optimal one pass large scale learning with averaged stochastic gradient descent", *arXiv preprint arXiv:1107.2490*, 2011.

[121] G Yin, "Stochastic approximation via averaging: The Polyaks approach revisited", in *Simulation and Optimization*, Springer, pp. 119–134, 1992.

[122] B. Zitova & J. Flusser, "Image registration methods: a survey", *Image and Vision Computing*, vol. 21, no. 11, pp. 977–1000, 2003.

Samenvatting

Optimaal gebruik van medische beeldgegevens vereist geavanceerde methodes voor beeldverwerking en beeldanalyse, bijvoorbeeld voor het berekenen van kwantitatieve biomarkers, het opstellen van anatomische en functionele modellen, het combineren van multimodale beelden en het vergelijken van baseline- en follow-up-beelden. Beeldregistratie is hierbij een essentiële techniek die dan ook breed wordt toegepast, zowel voor de ondersteuning van biomedisch onderzoek als in de klinische praktijk. In dit proefschrift presenteren we verbeteringen voor verschillende onderdelen van een registratieframework, met als doel de robuustheid, de nauwkeurigheid en de snelheid van de registratie te verbeteren. Onze specifieke bijdrages omvatten verschillende multi-resolutie-strategieën, transformatiemodellen en optimalisatiealgoritmes die worden gebruikt in beeldregistratie. Deze componenten hebben een directe invloed op de prestaties van het beeldregistratieframework.

Hoofdstuk 2 behandelt verschillende multi-resolutie-strategieën voor beeldregistratie. In een vergelijking met een conventionele, stapsgewijze, hiërarchische strategie worden verschillende nieuwe simultane multi-resolutie-strategieën gepresenteerd. Als in de optimalisatie de informatie van lage en hoge resolutieniveaus wordt gecombineerd, kunnen grootschalige en kleinschalige beeldinformatie gelijktijdig (simultaan) worden meegenomen. Op een soortgelijke manier kan een simultane multi-resolutiestrategie voor de transformatie worden gebruikt om de deformaties te verdelen over de verschillende resolutieniveaus van het transformatiemodel. Idealiter worden hierbij de grote deformaties gerepresenteerd op een grof transformatieniveau en worden de overgebleven kleinere deformaties gerepresenteerd op de fijnere transformatieniveaus. We hebben alle methodes geïmplementeerd met free-form deformations (FFD) in een B-spline-registratieframework [85]. De evaluatie-experimenten zijn uitgevoerd met publiek beschikbare long-CT-scans en T1-gewogen hersen-MRI-scans. De prestaties van de verschillende multi-resolutie-strategieën zijn vergeleken op zowel de nauwkeurigheid van de registratie als de gladheid van de transformatie. De resultaten laten zien dat een simultane multi-resolutiestrategie voor de beeld-data tot nauwkeurigere registraties leidt, en dat een hiërarchisch-simultane multi-resolutie-transformatiestrategie tot gladdere transformaties leidt. De afweging tussen registratienauwkeurigheid en transformatiegladheid hangt af van de toepassing, zodat we niet kunnen concluderen welke combinatie in het algemeen de voorkeur heeft. Uit onze experimenten blijkt echter dat de methode met een hiërarchisch-simultane transformatiestrategie en een simultane data-strategie op zowel registratienauwkeurigheid als transformatiegladheid beter presteert dan de traditionele hiërarchische registraties-

trategie.

In hoofdstuk 3 onderzoeken we of een FFD-model gebaseerd op wavelets voordelen biedt voor niet-rigide beeldregistratie. Met wavelets kan een signaal worden opgesplitst in verschillende schaalniveaus. Voor gebruik in een niet-rigide transformatiemodel moet een wavelet differentieerbaar zijn, compact gedragen en orthogonaal tussen verschillende schaalniveaus. Cai and Wang [13] hebben een waveletmodel in Sobolev-ruimte voorgesteld op basis van B-splines dat aan onze eisen voldoet. We gebruiken een nonlinear conjugate gradient (NCG)-optimizer [22,48] als optimalisatiemethode. In experimenten met 10 datasets met long-CT-scans en 18 datasets met T1-gewogen hersen-MRI-scans had het waveletmodel een grotere nauwkeurigheid dan het model met B-splines. Het transformatiemodel van het waveletmodel was ook gladder dan dat van het model met B-splines. In theorie hebben de wavelet- en B-spline-modellen dezelfde transformatieruimte, maar de experimentele resultaten waren toch verschillend. Een mogelijke verklaring hiervoor ligt in het preconditioning effect van de waveletparametrisatie, dat voor een impliciete regularisatie kan zorgen. Zonder aparte regularisatieterm kan het resultaat van de originele FFD-registratie bij kleinere knooppuntsafstanden slechter uitvallen. De wavelet-gebaseerde FFD-registratie lijkt in deze gevallen robuuster. Het kan interessant zijn om de wavelet-transformatie ook in combinatie met stochastische gradiënt descent (SGD) optimalisatiemethodes te evalueren. In de huidige implementatie is dit lastig, omdat de bepaling van de initiële stapgrootte in de veelgebruikte adaptive stochastic gradient descent (ASGD) methode in de huidige implementatie niet optimaal is voor gebruik in combinatie met het wavelettransformatiemodel, wat tot een lange rekentijd kan leiden. De snelle ASGD-optimizer uit [80] zou hiervoor mogelijk een oplossing kunnen bieden.

Hoofdstuk 4 onderzoekt het gebruik van lagere-orde B-splines. Geïnspireerd door de convolutionele definitie van B-splines stellen wij voor om door middel van een random perturbatieproces een n-de orde B-spline-transformatie te benaderen met een m-de orde B-spline, waarbij $m \leq n$. Deze nieuwe registratiemethode op basis van "randomly perturbed FFD" (RPFFD) wordt toegepast in een op SGD gebaseerd registratieframework [48]. Door een m-de orde B-spline te gebruiken in plaats van de oorspronkelijke n-de orde B-spline, worden de computationele kosten gereduceerd met een factor $(\frac{m+1}{n+1})^D$, omdat dankzij het kleinere draagvlak minder knooppunten nodig zijn voor de berekeningen. De registratienauwkeurigheid is gevalideerd in experimenten op gesimuleerde 2D hersenscans met gesimuleerde deformaties en een bekende ground truth. Publiek beschikbare 3D long-CT-scans en hersen-MRI-scans zijn gebruikt om de registratieresultaten op echte data te verifiëren. De methodes zijn vergeleken op registratienauwkeurigheid, transformatiegladheid en computationele efficiëntie. De experimentele resultaten laten zien dat de voorgestelde RPFFD-methode op registratienauwkeurigheid en transformatiegladheid beter presteert dan de standaard derde-orde FFD-methode. De computationele kosten van lagere-orde B-splines zijn zoals verwacht lager. Het is interessant om te zien dat de eerste- en tweede-orde B-splines met de random perturbation-techniek een vergelijkbare of zelfs betere registratienauwkeurigheid en transformatiegladheid kunnen bereiken dan de derde-orde B-splines. Mogelijke verklaringen voor dit resultaat worden besproken in de discussie van hoofdstuk 4.

Hoofdstuk 5 bespreekt een oplossing voor het probleem dat de optimalisatie van de beeldregistratie kan vastlopen in een lokaal minimum. Lokale minima in het optimalisatielandschap kunnen mogelijk worden geëlimineerd door de kostenfunctie glad te strijken. Multi-resolutie-strategieën bereiken dit deels indirect al doordat ze de afbeelding blurren, maar in onze aanpak onderzoeken we het effect van een directe smoothing van de kostenfunctie. Een conceptueel eenvoudige manier om dit te doen zou zijn om de kostenfunctie in de transformatie-parameterruimte te convolueren met een smoothing kernel. Dit is echter lastig vanwege de hoge dimensionaliteit van de parameterruimte. Geïnspireerd door [26] stellen wij daarom voor om tijdens het optimaliseren van de beeldregistratie Gaussische ruis toe te voegen aan de transformatieparameters. Anders dan bij het bewerkelijke multi-start-algoritme van [39], dat meerdere perturbaties toepast op de initiële transformatieparameters, worden bij onze methode in iedere iteratie slechts één of slechts enkele random perturbaties toegepast op de transformatieparameters. Deze randomized smoothing-techniek (RS) wordt gecombineerd met een SGD-optimizer [45], die gemakkelijk kan omgaan met de random perturbaties. De RS-techniek kan worden beschouwd als een computationeel efficiënte methode die impliciet de kostenfunctie gladstrijkt en op die manier de lokale minima uit het optimalisatielandschap verwijdert. In hoofdstuk 5 wordt de RS-techniek gevalideerd voor translatie-, rigide, affiene en niet-rigide B-spline-transformatiemodellen. De effectiviteit van de RS-registratiemethode is geëvalueerd in experimenten met synthetische tweedimensionale beelden, tweedimensionale cel-beelden en driedimensionale long-CT-scans en hersen-MRI-scans. De verbetering in registratieresultaten bewijst de effectiviteit van de RS-techniek.

In hoofdstuk 6 stellen we voor om tijdens de optimalisatie een constante stapgrootte te gebruiken (in plaats van een geleidelijk afnemende stapgrootte) in combinatie met een iteratieve middelingstechniek, om zo de convergentiesnelheid te verbeteren. In een SGD-optimalisatie wordt een stochastische benadering van de kostenfunctie gebruikt om in iedere iteratie de transformatieparameters bij te werken. Fouten in de stochastische benadering leiden tot randomness in de parameters. Convergentie moet daarom worden afgedwongen door de stapgrootte van de updates geleidelijk te verkleinen. Polyak en Juditsky [79] hebben bewezen dat de hoogste convergentiesnelheid kan worden bereikt door de parameters die door de SGD-optimizer worden verkregen te middelen over meerdere iteraties. Wij stellen daarom voor om een averaged SGD (Avg-SGD)-methode voor efficiënte beeldregistratie te gebruiken. Met de Avg-SGD-methode kan voor de optimalisatie een constante stapgrootte worden gebruikt, zonder aan registratieprecisie te verliezen. We bespreken twee varianten van de Avg-SGD-methode: een uitgestelde en een exponentiële variant. In de uitgestelde variant worden de eerste k_0 iteraties overgeslagen bij het berekenen van het gemiddelde. In de exponentiële variant wordt het gewicht van eerdere iteraties exponentieel verkleind, waardoor geen harde grens k_0 meer nodig is. De Avg-SGD-methode is geschikt voor zowel rigide als niet-rigide registratie. Experimenten met gesimuleerde 2D hersen-MRI-scans en echte 3D long-CT-scans demonstreren de effectiviteit van de Avg-SGD-methode in termen van convergentiesnelheid en registratieprecisie.

Samengevat introduceert dit proefschrift een aantal verbeteringen voor verschillende componenten van de registratiemethodologie. Alle voorgestelde nieuwe methodes zijn geëvalueerd in uitgebreide experimenten, met zowel synthetische data als

echte publieke biomedische data. De resultaten zijn vergeleken met die van state-of-the-art conventionele methodes.

De methodologische bijdrages zijn in principe onafhankelijk van elkaar, waardoor ze indien gewenst kunnen worden gecombineerd. Zo introduceert hoofdstuk 5 bijvoorbeeld de RS-techniek voor het onderdrukken van lokale minima in de kostenfunctie. Bij de RS-techniek wordt in iedere iteratie Gaussische ruis toegevoegd aan de transformatieparameters. Deze toegevoegde ruis vergroot de randomness van de SGD-optimalisatie en kan zo leiden tot een lagere precisie. Door tijdens de optimalisatie over meerdere iteraties te middelen, met behulp van de Avg-SGD-methode uit hoofdstuk 6, kan de versterkte ruis worden gecompenseerd, terwijl de convergentiesnelheid behouden blijft of zelfs kan worden vergroot. Hoofdstuk 5 laat zien dat het soms nodig is om in iedere iteratie over meerdere perturbaties te middelen om zo het effect van sterke Gaussische ruis te verminderen. De rekentijd van de registratie neemt echter direct toe met het aantal gemiddelden. Met de Avg-SGD-methode is daarentegen vrijwel geen extra rekentijd nodig. De gradiënt van de kostenfunctie hoeft niet vaker te worden geëvalueerd. Het middelen over de iteraties is geïmplementeerd met een efficiënte recursieve methode, zodat tijdens de optimalisatie slechts één extra vector met transformatieparameters hoeft te worden bewaard. Toepassing van de Avg-SGD-methode zorgt daardoor voor een substantiële vermindering in de rekentijd van de RS-techniek.

Als tweede voorbeeld: in hoofdstuk 2 wordt multi-level FFD gebruikt voor het modelleren van simultane multi-resolutie-strategieën. De hiërarchisch-simultane transformatie zorgt hierbij voor hogere computationale kosten. Dit kan mogelijk worden gecompenseerd met de nieuwe random perturbation-techniek uit hoofdstuk 4, waarmee hogere-orde B-splines kunnen worden benaderd met efficiëntere lagere-orde B-splines. Het randomly perturbed eerste-orde B-spline-model zou bijvoorbeeld kunnen worden gebruikt om in de hiërarchisch-simultane transformatie de multi-level B-spline FFD te modelleren. Op deze manier ontstaat een nieuwe registratiemethode die registratienauwkeurigheid en computationele efficiëntie combineert.

De methodes die worden gepresenteerd in dit proefschrift gebruiken geen domein-specifieke kennis en kunnen daarom voor veel verschillende toepassingen worden gebruikt. In dit proefschrift hebben we de resultaten van de voorgestelde registratiemethodes voornamelijk geëvalueerd op publieke CT- en MRI-scans. Het zou interessant kunnen zijn om de nieuwe technieken ook te evalueren met andere soorten medische beelden, zoals ultrasound en positron emission tomography (PET). De nieuwe methodes kunnen ook worden toegepast op andere anatomische structuren, zoals de lever, de prostaat et cetera.

In dit proefschrift beperken we ons tot het methodologische deel van de medische beeldregistratie. Uitgebreide klinische evaluaties en het in de praktijk toepassen van de voorgestelde registratiemethodes zijn een belangrijke richting voor toekomstig onderzoek. Om dit te faciliteren worden de nieuwe technieken publiek beschikbaar gemaakt als onderdeel van het open-source registratieprogramma `elastix`.

PhD Portfolio

Research

- PhD period: 2011–2015.

- Departments of Radiology and Medical Informatics, Erasmus MC.

- ASCI research school.

In-Depth Courses:

- Front-End Vision and Multi-Scale Image Analysis, ASCI, 2011.

- Advanced Pattern Recognition, ASCI, 2012.

- Knowledge Driven Image Segmentation, ASCI, 2012.

- Presentation Course, Erasmus MC, 2012.

- Summer School on Imaging in Neurology, EIBIR, 2013.

- Biomedical English Writing and Communication, NIHES, 2013.

- Computer Vision by Learning, ASCI, 2014.

International conferences:

- International Workshop on Biomedical Image Registration (WBIR), 2012.

- SPIE Medical Imaging (SPIE MI), 2014.

Other:

- Presentation at Dutch Society for Pattern Recognition and Image Processing (NVPHBV), 2012.

- Attendance at the Medical Imaging Symposium for PhD students (MISP), 2011, 2012, 2015.

- Presentations at the department seminar of the Biomedical Imaging Group Rotterdam.

- Presentations at the Medical Informatics Research Lunch.

International Conference Presentations:

- International Workshop on Biomedical Image Registration — WBIR 2012, Nashville, United States, July 7–8, 2012.

- SPIE Medical Imaging — SPIE MI 2014, San Diego, United States, February 15–20, 2014.

- *International Workshop on Biomedical Image Registration — WBIR 2014, London, United Kingdom, July 7–8, 2014.

- *International Conference on Medical Image Computing and Computer-Assisted Intervention — MICCAI 2014, Boston, United States, September 14–18, 2014.

*Due to circumstances I could not attend the conferences and give the presentation myself for WBIR 2014 and MICCAI 2014.

Reviewing for Journals:

- IEEE Transactions on Medical Imaging, IEEE Transactions on Image Processing, Pattern Recognition Letters, Optical Engineering, Computerized Medical Imaging and Graphics, Computers in Biology and Medicine, Journal of Medical Imaging and Health Informatics.

Teaching Assistant:

- Supervised a master student from ENSEEIHT, France, on *Stochastic gradient descent algorithm with Polyak averaging*, June 2014–September 2014.

Publications

Publications in International Journals:

- **W Sun**, W J Niessen and S Klein, "Randomly perturbed B-splines for nonrigid image registration", submitted.

- **W Sun**, DHJ Poot, I Smal, X Yang, W J Niessen and S Klein, "Stochastic optimization with randomized smoothing for image registration", submitted.

- **W Sun**, DHJ Poot, X Yang, W J Niessen and S Klein, "Averaged stochastic optimization for image registration", submitted.

- X Yang, J Pei and **W Sun**, "Elastic image registration using hierarchical spatially based mean shift", *Computers in Biology and Medicine*, vol. 43, no. 9, pp. 1086-1097, 2013.

- **W Sun**, W J Niessen, M van Stralen and S Klein, "Simultaneous multiresolution strategies for nonrigid image registration", *IEEE Transactions on Image Processing*, vol. 22, no. 12, pp. 4905-4917, 2013.

- **W Sun** and X Yang, "Nonrigid image registration based on control point matching and shifting", Optical Engineering, vol. 50, no. 2: pp. 027006, 2011.

- **W Sun** and X Yang, "Non-rigid registration using robust point matching with compactly supported radial basis function", Journal of Computational Information Systems, vol. 6, no. 9: pp. 2983-2989, 2010.

- **W Sun** and X Yang, "Image corner detection using topology learning", Journal of China Universities of Posts and Telecommunications, vol. 17, no. 6: pp. 101-105, 2010.

Publications in International Conference Proceedings:

- **W Sun**, W J Niessen and S Klein, "Free-form deformation using lower-order B-spline for nonrigid image registration", In *Medical Image Computing and Computer-Assisted Intervention - MICCAI, Lecture Notes in Computer Science*, vol. 8673, pp. 194-201, 2014.

- **W Sun**, W J Niessen and S Klein, "Randomly perturbed free-form deformation for nonrigid image registration", In *Biomedical Image Registration, Lecture Notes in Computer Science*, vol. 8545, pp. 62-71, 2014.

- **W Sun**, W J Niessen and S Klein, "Wavelet based free-form deformations for nonrigid registration", In *SPIE Medical Imaging*, pp. 90343N, 2014.

- **W Sun**, W J Niessen and S Klein, "Hierarchical vs. simultaneous multiresolution strategies for nonrigid image registration", In *Biomedical Image Registration 2012, Lecture Notes in Computer Science*, vol. 7359, pp. 60-69, 2012.

Conference Abstracts:

- **W Sun**, W J Niessen and S Klein, "Hierarchical vs. simultaneous multiresolution strategies for nonrigid image registration", In *Dutch Society for Pattern Recognition and Image Processing (NVPHBV)*, 2012.

Acknowledgment

I came to Netherlands and started my PhD journey in 2011. It was a profound and exciting change in my life. After four years intensive PhD life, Im very glad to report my findings in this thesis. All of my achievements cannot be obtained without the helps and encouragements from my supervisors, colleagues, friends and family members.

I would like to thank my promotor Prof.dr. Wiro Niessen and copromotor Dr.ir. Stefan Klein for providing me this unique opportunity to pursue my PhD under your supervision. Im deeply impressed and influenced by Wiros vision and passion in scientific research. You are the person who offers me this top-level platform to carry out my research in image registration. Wiro you are an ideal model in my research life. Stefan you are the best daily supervisor for sure. I learned a lot from your noble personality and rigorous attitude. You always save me from the dead end and guide me to the right track. I hope I can still practice your virtues in living and doing research in my future life. Please send my gratitude to Magda as well.

Here, I want to acknowledge my inner doctoral committee: Dr.ir. J. van den Bosch, Dr.ir. F.M. Vos, Prof.dr. D. Rueckert and plenary doctoral committee: Dr.ir. T. van Walsum, Prof.dr. G.C. van Rhoon, Dr.ir. Jef Vandemeulebroucke for reviewing my thesis and attending to my defense.

Dirk and Jean-Marie thank you for being my paranymphs. As an amiable and insightful coauthor, Dirk I hope we can continue our collaboration in future. Jean-Marie I wont forget our joyful time together. You are also the living map during our sports. I was inspired by your opinions many times.

I want to thank my colleagues and friends in research. I participated in three research groups in BIGR and acquired a lot of knowledge in different aspects in medical image analysis. Dirk, Esther, Annegreet, Marius, Marcel, Hakim, Wyke, Carolyn, Gennady, Eugene, Veronika and Joor I learned quite some knowledge about machine learning, connectome, MRI imaging, genetics and pipeline from your work. For the image guided intervention, Theo, Nora, Gerardo, Pierre, Jyotirmoy, Luu, Guillaume, Hua, Roman and Reinoud, thanks for sharing your expertise and knowledge. In the RAMBO group with the colleagues from LUMC, Stefan, Marius, Diego, Jean-Marie, Wyke, Gokhan, Yuchuan, Floris, Zhuo, Kasper, Gorkem and Hessam thank you for the discussions in image registration. I really enjoy the time in LUMC. I also would like to thank Andres for the pleasant time together. Gijs thanks for the help with my Dutch summary. Ihor thanks for the useful contribution to our collaborative work. Miro I really enjoy the time we spent together. Ghassan thanks for bring us a lot of

laugh. Marco thanks for the talk and dinner. It is nice to meet Marleen, Henri, Erik, Jifke, Emilie, Mart, Erwin, Adria, Zahra in BIGR.

Hua, Yao and Chaoping thanks for the happy time together. I feel lucky to have you in our group. I want to thank Desiree, Petra and Carmen for your helps in documents. I also want to take this opportunity to thank my former colleagues Valerio, Arna, Henk, Esben, Rahil, Ruben, Hui, Lin, Yuan, Xueyang, Jian, Coert, Renske, Azadeh and Michiel. It was nice to meet you in Netherlands.

Thank you Eugene for introducing me many friends in Den Haag. CT, Yunting, Mey thank you for the pleasant time and dinners together. Jiajie and Yu I really enjoy the time with you. Shuqi and Nana you are very nice persons.

It was a lot of fun time with my friends in Erasmus MC and Netherlands. Yanwei, Wenting, Jingjing, Baoyue, Haibo, Zhouqiao, Ruxi, Qiushi, thank you for your helps and having a lot of fun with you. It is wonderful to meet Zhichao, Tao, Bin, Shihao, Changbin, Shan, Kuikui, Wen, Ya, Kaiyin, Fan, Bei, Ruoyu, Yannan, Bo, Zhanmin, Yingying, Xiaolei, Yibing, Wenjie, Qing and other friends in EMC and Rotterdam.

Yuchuan thanks for your helps in my research and life. I hope we can still find some other topics to work together in future. Jiong and Zhuo I enjoy the time with you. I also want to thank other friends in Leiden Shengnan, Xinpei, Zhiwei, Yingguang and Qing.

I would like to thank Prof. Xuan Yang and Prof. Jihong Pei. Prof. Yang you opened the door of image registration to me. Without your supports, I could not finish my PhD.

Last, I want to express my gratitude to my family. My parents and grandmother thank you for the consistent supports in my career. Due to the PhD research, I havent seen you in person for very long time. My dear wife Qiye we met and got married in Netherlands. My life wouldn't be so colorful without you. We shared our happy and hard time together in the past years. I really appreciate your understanding and supports as always. Meanwhile, I would like to thank my parents-in-laws for your love and care to Qiye and me. I want to thank Qiwei and Jing for your helps and encouragements in our life in Netherlands. My special thanks also go to my uncle, aunt and Yan.

Curriculum Vitae

Wei Sun was born in Xi'an, China in 1984. After high school he has started studying Computer science at the Xidian university in Xi'an. He has taken his bachelor's degree in 2006 presenting a project about online system of course management.

After that he went to industry as a software engineer for two years in Shenzhen, China. During that time, he participated in developing an enterprise resource planning solution.

In 2008 he continued his study as an MSc student at Shenzhen university in China and received his master degree three years later. During the master period, he participated in a project about nonrigid image registration based on control point matching and published three international journal papers.

From 2011 until 2015, Wei Sun worked as a Ph.D. student at the Biomedical Imaging Group Rotterdam, Erasmus MC, Netherlands. There he developed novel methods for stochastic image registration, resulting in this thesis.